






The immunomodulatory ballet of tumour-derived extracellular vesicles and neutrophils orchestrating the dynamic CD73/PD-L1 pathway in cancer

Dominique S. Rubenich^{1,2,3}  | Jordana L. Domagalski³  | Gabriela F. S. Gentil³  |
Jonas Eichberger^{1,2} | Mathias Fiedler^{1,2} | Florian Weber⁴ | Marianne Federlin⁵ |
Hendrik Poeck^{6,7} | Torsten E. Reichert¹ | Tobias Ettl¹ | Richard J. Bauer^{1,2} |
Elizandra Braganhol³  | Daniela Schulz^{1,2} 

¹Department of Oral and Maxillofacial Surgery, University Hospital Regensburg, Regensburg, Germany

²Department of Oral and Maxillofacial Surgery, Experimental Oral and Maxillofacial Surgery, Center for Medical Biotechnology, University Hospital Regensburg, Regensburg, Germany

³Biosciences Graduate Program, Federal University of Health Science of Porto Alegre (UFCSPA), Porto Alegre, Brazil

⁴Institute of Pathology, University of Regensburg, Regensburg, Germany

⁵Department of Conservative Dentistry and Periodontology, University Medical Center Regensburg, Regensburg, Germany

⁶Clinic and Polyclinic for Internal Medicine III, University Hospital Regensburg, Regensburg, Germany

⁷Leibnitz Institute for Immunotherapy (LIT), Regensburg, Germany

Correspondence

Daniela Schulz, Department of Oral and Maxillofacial Surgery, University Hospital Regensburg, Franz-Josef-Strauss Allee 11, 93053 Regensburg, Germany.
Email: daniela.schulz@ukr.de

Funding information

Deutsche Forschungsgemeinschaft, Grant/Award Numbers: DFG, GZ: 3696/7-1; Coordenação de Aperfeiçoamento de Pessoal de Nível Superior, Grant/Award Number: 88881.895087/2023-01; Conselho Nacional de Desenvolvimento Científico e Tecnológico, Grant/Award Number: 142520/2020-9; Deutscher Akademischer Austauschdienst, Grant/Award Number: 57705675

Abstract

Head and neck squamous cell carcinoma (HNSCC) is a global cancer burden with a 5-year overall survival rate of around 50%, stagnant for decades. A tumour-induced immunosuppressive microenvironment contributes to HNSCC progression, with the adenosine (ADO) pathway and an upregulated expression of inhibitory immune checkpoint regulators playing a key role in this context. The correlation between high neutrophil-to-lymphocyte ratio (NLR) with advanced tumour staging suggests involvement of neutrophils (NØ) in cancer progression. Interestingly, we associated a high NLR with an increased intracellular PD-L1 localization in primary HNSCC samples, potentially mediating more aggressive tumour characteristics and therefore synergistically favouring tumour progression. Still, further research is needed to harness this knowledge for effective treatments and overcome resistance. Since it is hypothesized that the tumour microenvironment (TME) may be influenced by small extracellular vesicles (sEVs) secreted by tumours (TEX), this study aims to investigate the impact of HNSCC-derived TEX on NØ and blockade of ADO receptors as a potential strategy to reverse the pro-tumour phenotype of NØ. UMSCC47-TEX exhibited CD73 enzymatic activity involved in ADO signalling, as well as the immune checkpoint inhibitor PD-L1. Data revealed that TEX induce chemotaxis of NØ and the sustained interaction promotes a shift into a pro-tumour phenotype, dependent on ADO receptors (PIR), increasing CD170^{high} subpopulation, CD73 and PD-L1 expression, followed by an immunosuppressive secretome. Blocking A3R reduced CD73

This is an open access article under the terms of the [Creative Commons Attribution-NonCommercial-NoDerivs License](https://creativecommons.org/licenses/by-nc-nd/4.0/), which permits use and distribution in any medium, provided the original work is properly cited, the use is non-commercial and no modifications or adaptations are made.

© 2024 The Authors. *Journal of Extracellular Vesicles* published by Wiley Periodicals, LLC on behalf of the International Society for Extracellular Vesicles.

and PD-L1 expression. Co-culture experiments with HNSCC cells demonstrated that TEX-modulated NØ increase the CD73/PD-L1 axis, through Cyclin D-CDK4/6 signalling. To support these findings, the CAM model with primary tumour was treated with NØ supernatant. Moreover, these NØ promoted an increase in migration, invasion, and reduced cell death. Targeting PIR on NØ, particularly A3R, exhibited potential therapeutic strategy to counteract immunosuppression in HNSCC. Understanding the TEX-mediated crosstalk between tumours and NØ offers insights into immunomodulation for improving cancer therapies.

KEYWORDS

adenosine signalling, biomarker, cytoplasmic PD-L1, exosome, head and neck squamous cell carcinoma, immune checkpoint resistance, tumour-associated neutrophils (TAN)

1 | INTRODUCTION

Head and neck squamous cell carcinoma (HNSCC) is a prevalent form of cancer, with approximately 600,000 new cases reported worldwide annually (Sung et al., 2021). Despite extensive research and novel therapeutic approaches, the 5-year overall survival rate for HNSCC patients has stagnated at around 50% for decades (Leemans et al., 2018).

Tumour cells use various mechanisms to induce and sustain a favourable chronic inflammatory environment, abundant in soluble factors that promote their own proliferation and survival (Giuliani et al., 2021). The tumour microenvironment (TME) in HNSCC is characterized by significant immune alterations, often leading to an immunosuppressive niche, promoting tumour growth, invasion, and immune evasion and thereby challenging effective treatment (Elmusrati et al., 2021). Immune checkpoint molecules like PD-L1 are frequently overexpressed in a variety of tumour entities and provide a promising target for antibody-based PD-1/PD-L1 immunotherapy (Mortezaee, 2020). Despite some encouraging outcomes, immune checkpoint inhibition in HNSCC often yields limited improvement or even hyperprogression (Ettl et al., 2022). The heterogeneity of PD-L1 expression and the lack of reliable biomarkers still leads to unpredictable outcomes (Zhou et al., 2020). There is increasing evidence that PD-L1 expression as well as its subcellular localization is highly dynamic (Schulz et al., 2021) and also mediates tumour cell-intrinsic functions that may trigger tumour-promoting effects (Eichberger et al., 2020; Gato-Cañas et al., 2017).

Interestingly, there is emerging new research targeting CD73 and PD-L1 as a potential combination therapy, addressing two immunosuppressive tumour escape strategies at the same time (Allard et al., 2019; Demeules et al., 2022; Ye et al., 2023). The adenosine (ADO) pathway in HNSCC is acknowledged as a major contributor to tumour-mediated immunosuppression and tumour progression (Deng et al., 2018). ADO is produced within the TME mostly through the enzymatic breakdown of ATP through the activity of the ectonucleotidases NTPD1 (CD39) and NT5E (CD73). Extracellular ADO contributes to immunosuppression. It serves as a potent signalling molecule that activates ADO receptors (PIR), A1, A2_A, A2_B and A3, thereby modulating crucial cellular processes including differentiation, cell death and triggering an immunomodulatory response (Allard et al., 2017).

Also, the presence of immunosuppressive immune cells such as regulatory T cells (Tregs) and myeloid-derived suppressor cells (MDSCs) can hinder the tumour immune response (Elmusrati et al., 2021). The myeloid infiltrate is a crucial component of the TME and significantly influences its progression (Zhang et al., 2018). Emerging evidence suggest a pivotal role of tumour-associated neutrophils (TANs) in the interplay between tumour and TME (Carus et al., 2013; Rubenich et al., 2023). TANs are phenotypically modulated neutrophils (NØ) and, consequently, contribute to the perpetuation of the disease (Haas & Obenauf, 2019). NØ modulation have been shown to adapt according to tissue environment, and recently have been proposed the importance of tumour-derived extracellular vesicles (TEX) as main characters in tumour crosstalk.

Small extracellular vesicles (sEVs) have garnered significant attention for their potential role in facilitating intercellular communication. These sEVs, also known as exosomes, represent a distinct subset of extracellular vesicles originating from multivesicular bodies (MVBs) and typically measure between 30 and 150 nm in diameter. Particularly intriguing are their unique biogenesis process and surface membrane composition, which closely mirrors those of their parental cells (Gurunathan et al., 2019). Importantly, the cargo carried by sEVs can vary depending on the specific microenvironment. There is evidence to suggest that TEX, have the capacity to modulate the phenotype and functional behaviour of NØ, influencing their immune responses (Rubenich et al., 2021).

In our present study, we show that tumour progression and the neutrophil-to-lymphocyte ratio (NLR) correlate with intracellular PD-L1 localization in tumour cells. Furthermore, we examined the ability of HNSCC-derived TEX to chemoattract and interact with NØ resulting in an induction of an immunosuppressive phenotype in NØ, thus promoting cancer progression. In addition, blocking ADO receptors can reverse the NØ pro-tumour phenotype. TEX-modulated pro-tumour NØ

demonstrated different influence on tumour progression between four cell lines; however, an important similar pattern of increasing CD73/PD-L1 axis expression in tumour cells, may indicate their role in immunosuppressive TME.

2 | MATERIALS AND METHODS

HNSCC patient cohort: Patient recruitment for primary HNSCC tissue samples, as well as the retrospective database analysis were conducted at the Department of Oral and Maxillofacial Surgery of the University Hospital Regensburg. Seventy-six patients with HNSCC of various localizations were included in the study cohort. The patients were diagnosed and staged between 2016 and 2023 at the Department of Oral and Maxillofacial Surgery, University Hospital Regensburg. Clinical and histopathologic data as well as neutrophil and lymphocyte counts were collected from patients' medical records. All participants involved in this study were thoroughly informed about the nature and purpose of the study, as well as the procedures involved. Written informed consent was obtained from all individual participants involved in the study prior to sample collection. Ethical approval for this study was granted by the Ethics Committee at University Hospital Regensburg (n° 16-299-101). All procedures performed in this study involving human participants were conducted in compliance with the ethical standards of the institutional research committee and with the 1964 Helsinki Declaration and its later amendments or comparable ethical standards.

Immunohistochemistry (IHC) of HNSCC patient samples: Formalin-fixed, paraffin-embedded tumour tissue was obtained from the archive of the Institute of Pathology at the University of Regensburg. From each block of samples, 3 µm thick sections were cut from the tumour centre and tumour periphery. Sections were mounted on SuperFrost Plus microscope slides (R. Langenbrinck Labor- u. Medizintechnik, Emmendingen, DE). IHC single-staining was performed for CD66b and PD-L1. IHC double-staining was performed for FoxP3 and CD3, following the standard protocol of the Institute of Pathology, University of Regensburg, using a BenchMark Ultra IHC/ISH system (Ventana Medical Systems, Inc, Tucson, AZ). Anti-CD66b (ab300122, Abcam, Cambridge, UK), anti-FOXP3 (14-4777-82, clone 236 A/E7, eBioscience, Thermo Fisher Scientific, San Diego, CA), anti-CD3 (A 0452; Dako GmbH, D), anti-PD-L1 (human PD-L1, clone 28-8, ab205921, Abcam), anti-PD-L1 (human PD-L1, clone EIL3N, #13684, Cell Signaling Technology, Danvers, MA, USA) and anti-PD-L1 (human PD-L1, clone 22C3, M3653, Dako GmbH) were used as primary antibodies. The Dako REAL Envision Detection System, Peroxidase/DAB+, Rabbit/Mouse (Dako, Glostrup, DK) was utilized for detection. Hematoxylin solution was used for counterstaining. Morphological staining with appropriate hematoxylin and eosin was performed as controls for all samples. PD-L1 membranous and cytoplasmic staining was observed on both immune and epithelial cells. Staining intensity was not considered in the scoring process, and evaluations of immune and tumour cells were conducted separately. The absolute number of intratumoral cells stained on the membrane in a high-power field (HPF) at 400-fold magnification was counted for CD3, FoxP3 and CD66b. The relative number of tumour cells stained on membrane and cytoplasm were counted for PD-L1⁺ and the absolute number of CD66b⁺, CD3⁺ and FoxP3⁺. The HPF represents the area of the tumour where most of the cells of interest are located. The evaluation area at 400-fold magnification corresponded to a rectangle with a height of 256 µm and a width of 432 µm for the microscope used to achieve the highest possible reproducibility. Counting was performed manually by an experienced pathologist.

Primary human neutrophil isolation: Peripheral blood was obtained from healthy volunteers, using EDTA blood collection tubes (S-Monovette, Sarstedt AG & Co. KG, Nümbrecht, DE) and processed within 15 min following a protocol previously described (Oh et al., 2008). For all further assays, neutrophils cultivated in non-conditioned EDHI-FBS media were used as internal control. The institutional ethics review board of the University Hospital Regensburg (n° 20-1990-101) approved this study.

HNC cell lines: The human head and neck cancer cell line UMSCC47 (SCC47) was purchased from ATCC (Manassas, VA, USA). The human head and neck cancer cell lines FaDu (RRID: CVCL_1218) and SCC9 (RRID: CVCL_1685) were ordered from ATCC (Manassas, VA, USA) as part of the Head and Neck Panel TCP-1012. The human head and neck cancer cell line PCI52 (RRID: CVCL_RJ99) was kindly provided by Prof. Dr. Theresa. L. Whiteside (University of Pittsburgh Cancer Institute (PCI), Pittsburgh, PA, USA) in 2013 (Lin et al., 2007). Authentication of PCI52 was performed by the Leibniz Institute German Collection of Microorganisms and Cell Cultures (DSMZ), Berlin, DE) via STR-DNA-typing using nonaplex PCR [A1806475-1].

Culture conditions for cell lines: Cells were cultured at 37°C under controlled conditions with 5% CO₂. The culture medium DMEM (PAN-Biotech, Aidenbach, DE) was supplemented with 1% L-glutamine (Sigma-Aldrich, St. Louis, MO, USA), 100 units/litre (U/L) penicillin/streptomycin 0.5 U/L (Sigma-Aldrich) and 10% foetal bovine serum (FBS) (Gibco, Carlsbad, CA, USA). The medium was changed every 2 to 3 days, and the cells were passaged prior to reaching confluence. Detachment of cells was achieved by incubation with Accutase solution (Sigma-Aldrich) for 5 to 10 min at 37°C.

Tumour spheroids: Spheroids were generated with the hanging drop technique. Per drop, 2 × 10⁴ cells were seeded in 30 µL cell culture medium, including 0.12% methylcellulose (Sigma-Aldrich), onto the inner part of the lid form a petri dish (Sigma-Aldrich). After seeding, the lid was carefully turned, and the petri dish closed. The cells formed 3-dimensional (3D) spheroids overnight at 37°C under controlled conditions with 5% CO₂. A volume of 10 mL phosphate buffered saline (PBS) in the lower part of the petri dish prevented the drops from drying out.

TEX isolation: For TEX isolation the culture medium DMEM (PAN-Biotech) was supplemented with 1% L-glutamine (Sigma-Aldrich), 100 units per litre (U/L) penicillin/streptomycin 0.5 U/L (Sigma-Aldrich) and 10% sEV-depleted heat-inactivated foetal bovine serum (EDHI-FBS) (Gibco, Carlsbad, CA, USA). Depletion was achieved by ultracentrifugation at 100,000 relative centrifugal force (rcf) for 3 h. A number of 2.5×10^6 cells were cultured in 150 cm² cell culture flasks (Greiner Bio-One, Kremsmünster, AT), containing a total volume of 25 mL culture medium. After 72 h of incubation, the supernatants were carefully collected for further TEX isolation. 50 mL of SCC47 cell culture supernatant underwent a two-step centrifugation at room temperature (RT) for 10 min at 2000 rcf, followed by 10,000 rcf at 4°C for 30 min. Subsequently, the supernatants were filtered through a 0.22 µm bacterial filter (Millex-GP, Sigma-Aldrich) attached to a 50 mL syringe (BD Plastipak). Using Vivacell 100 concentrators and a centrifugal force of 4000 rcf, the filtered supernatants were concentrated down to 1 mL volume.

TEX characterization: TEX were isolated using the mini-size exclusion chromatography (mini-SEC) method, following the previously described protocol in (Ludwig et al., 2019). A volume of 1 mL of fraction #4 was collected throughout the Sepharose CL-2B (17014001, Cytiva, SE) column for further characterization. TEX protein concentration was determined by using a BCA protein assay (Pierce Biotechnology, Rockford, IL, USA). Tunable resistive pulse sensing (TRPS) was employed to assess the concentration and size distribution of particles in fraction #4. The assessment involved a NP100 nanopore at a 45.05 mm stretch, 0.64 V, and a 17 mbar. Samples were calibrated using 114 nm carboxylated polystyrene beads at a concentration of 2×10^{11} particles/mL. Data were recorded and analysed with version 3.2 of the IZON software (<http://www.izon.com>). The results provided particle concentrations as the number of particles within fraction #4. Images were taken with scanning electron microscopy (SEM), low vacuum (LV) mode was utilized with energy-dispersive x-ray spectroscopy and proximity ligation assay techniques. The SEM was operated at a voltage of 4 kV with Spot 3, while maintaining a working distance of 10 mm and a pressure of 1.5 Torr. The aperture size was set to 6 for imaging purposes.

Neutrophil treatment with TEX and ADO signalling antagonists: For TEX-treated groups, a concentration of 10 µg of TEX / 10^6 neutrophils (NØ) was added. The amount of TEX used in this setup was assessed via concentration curve. Lower tested amounts of TEX (1, 5, 7 µg) didn't show any significant effect (data not shown). The following antagonists were used to block ADO signalling: AMPCP (CD73 inhibitor—100 µM, Tocris), CGS15943 (P1 antagonist—0.1 µM, Tocris), PSB36 (A1R antagonist—1 µM, Tocris), SCH442416 (A2A R antagonist—1 µM, Tocris), MRS1754 (A2B R antagonist—1 µM, Tocris) and PSB10 hydrochloride (A3R antagonist—1 µM, Tocris, UK). The control group only included NØ. For further information about primary healthy NØ, see Figure S1. NØ viability was assessed using the specified compound concentrations. No notable impact on NØ viability was observed.

Extracellular adenosine quantification: After 48 h, the supernatant from seven different biological experimental samples from each group: NØ CTRL, NØ with 10 µg TEX, and NØ treated with CD73 inhibition (AMPCP) and TEX, were evaluated through Human Adenosine ELISA Kit (MBS2605344, MyBiosource, San Diego, CA, USA) according to manufacturer's instructions. Briefly, 100 µL of each sample was added in duplicates, absorbance was measured with 450 nm and the concentration values (ng/mL) were calculated with the standard curve equation.

Neutrophil transmigration assay: A 48-well plate was used containing NØ (10^6 /mL) in the upper chamber with 3 µm micropore (662630, Greiner Bio-One), both with and without AMPCP and CGS15943 treatments. The lower chamber held PBS 1× and FBS as negative and positive controls respectively, while 10 µg TEX, diluted in DMEM ØFBS were used for the experimental groups. After incubation at 37°C with 5% CO₂ for 3 h, migrated cells from the lower chamber were harvested. NØ counts were obtained using Neubauer's chamber, and results, normalized with the positive control to eliminate donor variability, are presented as percentage of NØ (Chen et al., 2006).

Neutrophil-TEX imaging: (1) *Scanning electron microscopy (SEM):* NØ w/ and w/o TEX were treated with 2.5% glutaraldehyde (Sigma-Aldrich) in Soerensen buffer for fixation. Post-fixation, the samples were rinsed with distilled water and dehydrated through an ascending alcohol series with 10%, 30%, 50%, 70% and 90% ethanol (Sigma-Aldrich) for 10 min each, followed by three cycles in 100% alcohol, for 20 min each. The generated pellet was mixed with propylene oxide (Sigma-Aldrich), carefully dropped onto a stub with a coverslip, and air-dried for 30 min. Subsequently, the sample was sputter-coated with platinum for 40 s, using a working distance of 50 mm and a current of 30 mA. SEM settings were as follows: high voltage (HV), electron detector (EDT), 4 kV accelerating voltage, spot size 3 and a working distance of 10 mm. (2) *Immunofluorescence (IF):* TEX were labelled with SYTO RNaselect (1:50, S32703, Invitrogen, Massachusetts, USA) prior to isolation. After 4 h, samples were fixated with 4% paraformaldehyde (Merck), followed by Alexa Fluor 546 Phalloidin (A22283, Invitrogen) and VECTASHIELD Antifade Mounting Medium with DAPI (A-1200, Vector Laboratories, Inc., Newark, USA) staining. Photos were taken in magnification of 40-fold, to visualize TEX-NØ interactions. For NØ-TEX imaging, NØ were incubated with TEX for 4 h. A deeper impact in the retention of TEX in the presence of the studied compounds was not further investigated.

Neutrophil phenotype characterization: After 48 h incubation, NØ were evaluated using the BD LSRFortessa Cell Analyzer (BD, Franklin Lakes, NJ, USA). The CD11b⁺ (1:50, 557754, BD)/CD66b⁺ (1:100, 562254, BD) were used as NØ markers, following CD170^{low} for anti-tumour phenotype and CD170^{high} (1:20, 564371, BD) for pro-tumour phenotype, as described in Jaillon et al. (2020). Next, the mean fluorescent intensity (MFI) of CD73 (1:20, 561258, BD) was tested in both phenotypes. Furthermore, the expression of PD-L1 was evaluated by western blotting (WB), using an anti-PD-L1 antibody (clone EIL3N, #13684, Cell Signaling Technology).

Secretome analysis: After 48 h incubation, supernatants from non-treated (CTRL) and TEX-treated NØ were collected. We pooled five different biological experiments in each group. Using 10 µL containing 5 µg of protein each resulted in a cumulative protein amount of 25 µg per group. Each group was analysed for the expression of 36 different cytokine-related proteins using the Human Cytokine Array Kit (ARY005B—Proteome Profiler, R&D Systems, Minneapolis, MN, USA), following the manufacturer's instructions.

Subcellular protein fractions: HNSSC tissue was fractionated with the Subcellular Protein Fractionation Kit for Tissues (Thermo Scientific, Waltham, MA, USA) according to the manufacturer's instructions. A tissue weight of 100–200 mg was used for each sample. Tissue was washed gently with ice-cold PBS. Excess liquid was removed. Tissue was cut into small pieces and placed in a pre-chilled tube for homogenization with a pestle (Kisker Biotech GmbH & Co. KG) in CEB-buffer. For removal of tissue debris, the homogenized tissue was transferred into the Pierce Tissue Strainer (Thermo Scientific) before performing the subcellular fractionation. Protease inhibitors (Halt Protease Inhibitor Cocktail 100×, Thermo Scientific) were added to each buffer to maintain integrity. All incubations were performed at 4°C unless otherwise noted. For long-term storage, fractions were stored at –80°C.

Western blot analysis: For SDS-PAGE, 10% agarose gels were loaded with 10 µg protein of fraction #4 or 20 µg of total protein lysate/fractionated proteins and transferred to a PVDF membrane. Membranes were incubated overnight at 4°C with primary antibodies. Primary antibodies for TEX characterization: anti-Calnexin (ab133615, Abcam), anti-HSP70 (ab181606), anti-CD9 (ab92726, Abcam), anti-TSG101 (ab125011, Abcam), anti- α -Tubulin (200-301-880, Rockland Immunochemicals, Philadelphia, USA). Primary antibodies for purinergic signalling: anti-CD73 (ab133582, Abcam), anti-CD39 (223842, Abcam). Primary antibodies for primary tumour characterization: anti-PD-L1 (#13684, Cell Signaling Technology, Danvers, MA, USA (CST)), anti-PD-L1 (#51296, CST), anti-PD-L2 (#83723, CST), anti PD-1 (#86163, CST), anti-EGF Receptor (#4267, CST), anti-Vimentin (#5741, CST), anti-E-cadherin (610182, BD), anti-N-cadherin (610921, BD), anti-Twist (sc-81417, Santa Cruz Biotechnology, Dallas, TX, USA), anti-Snail (sc-393172, Santa Cruz Biotechnology), and anti-CD44 (#3570, CST), anti-VEGFR2 (#9698, CST), anti-VEGF (NB10023832, Novusbio, Uppsala, Sweden). Primary antibodies for analysis of the CD73/PD-L1 signalling cascade: anti-CDK6 (#3136, CST), anti-Cyclin D1 (#55506, CST). Anti- β -actin (ab8227, Abcam) was used as the loading control. Secondary antibody Goat anti-rabbit (32460, Invitrogen, Waltham, MA, USA) or anti-mouse (32430, Invitrogen) when appropriate (Théry et al., 2018). For signal detection SuperSignal West Femto substrate (34096, Thermo Scientific Waltham, MA, USA) was used. Colorimetric and chemiluminescent images were processed using the high-resolution, high-sensitivity ChemiDoc XRS+ Imaging System (Bio-Rad, Hercules, CA, USA). Equal loading of proteins was confirmed with Ponceau S (SERVA Electrophoresis GmbH, Heidelberg, DE) total protein staining. The analysis was carried out using Image Lab software 6.0.1 (Bio-Rad).

Chicken embryo chorioallantoic membrane (CAM) assay: Fertilized chicken eggs were acquired from an organic farmer (Herkner, Neutraubling, DE). They underwent a careful incubation process at 37.5°C and 63% humidity in a ProCon egg incubator (Grumbach, Aßlar, DE) for a period of 3 days, with regular rotation every 30 min. After that, a small window was cut in the eggshell and securely sealed using Durapore (1538-1, 3 M, Saint Paul, MN, USA). On Day 7, a piece of HNSSC primary tumour (PT) obtained from surgery of tumour resection (~30 µg was added to the top, followed by the addition of 60 µL of NØ supernatant from the following groups ($n = 5$): PT, DMEM vehicle control; +NØ, secretome from healthy NØ; +TEX, secretome from TEX-modulated NØ; +CGS15943, secretome from pre-treated NØ with CGS15943, followed by TEX incubation. This treatment was repeated for three consecutive days. The experiment concluded on Day 14 when the tumour was collected and lysed for WB evaluation of the proteins PD-L1, CD73 and CDK6 as previously described.

Co-cultivation of NØ, TEX and tumour cells: A number of 1×10^6 NØ was pre-treated with 10 µg TEX for 24 h, as described. Afterward, the primed NØ were added to tumour cells for functional assays. The number of tumour cells was determined by the functional assay. For the proliferation and apoptosis assays 3000 adherent tumour cells were seeded into a 96-well plate, for the spheroid spreading assay one tumour spheroid consisting of 20,000 tumour cells was seeded into a 96-well plate. After 48 h of co-cultivation, the NØ were washed out from the tumour cells to eliminate any NØ interference with subsequent enzymatic assays or the tumour cell protein lysate.

Proliferation assay: Cell proliferation was measured using CellTiter 96 AQueous One Solution Cell Proliferation Assay (MTS—Promega, Wisconsin, USA). Therefore, 3000 tumour cells were seeded onto a 96-well plate (Greiner Bio-One) overnight. Proliferation was measured 48 h after treatment according to the manufacturer's instructions.

Apoptosis assay: Apoptosis was measured using Apo-ONE Homogeneous Caspase-3/7 Assay (Promega). Therefore, 3000 tumour cells/well were seeded onto a 96-well plate (Greiner Bio-One) overnight. Apoptosis was measured 48 h after treatment according to the manufacturer's instructions.

Live-cell imaging wound healing assay: To analyse cell migration, 1×10^5 tumour cells were seeded onto a 96-well plate (Greiner Bio-One) overnight. After the scratch, cells were washed two times with PBS. After treatment, cell migration in serum-reduced culture medium (5% FBS) was observed for 48 h using live-cell imaging (Axio Observer Microscope, Zeiss, Oberkochen, DE) with an imaging interval of 1 picture/h at 40-fold magnification (ZENpro software, Zeiss). Afterward, the wound healing progress was quantified at 0, 5, 10, 12, 15 and 18 h after treatments by area measurement using Fiji ImageJ.

Spheroid spreading assay: To analyse cell spreading, one spheroid per 96-well (Greiner Bio-One) was seeded in 50 µL DMEM. Two hours after seeding, pictures of the attached spheroids were taken and defined as the starting point of the experiment (0 h).

Images were taken with 2-fold magnification. Right after, cells were treated. The final volume was 100 μL of serum-reduced culture medium. Again, 48 h after treatment pictures of spread spheroids were taken with the same magnification (48 h). For subsequent WB analysis, tumour cells were lysed in radio-immunoprecipitation buffer (RIPA) buffer including protease inhibitors (Complete Mini Protease Inhibitor Cocktail) (Roche Diagnostics, Basel, CH). For quantification of the spread area, the diameter was measured with the ImageJ software and the change in the size of the area covered by cells was calculated. Therefore, the ratio of the area after 48 h to the covered area after seeding (0 h) was calculated and referred to as the spreading ratio. Statistical analysis was performed using the GraphPad Prism 9 software (GraphPad Software, San Diego, CA, USA).

Statistical analysis: Data are presented as mean \pm SD. Two-way analysis of variance (ANOVA) followed by Tukey–Kramer post-hoc test was performed or one-way ANOVA with Bonferroni's test, when appropriate. For the correlation of NLR with intracellular PD-L1, the Pearson test correlation matrix was performed to analyse the strength of the association. Correlation was interpreted as follow: weak 0.1–0.3 (positive); -0.1 to -0.3 (negative); medium 0.3 to 0.5 (positive); -0.3 to -0.5 (negative); strong (0.5 to 1.0 (positive); -0.5 to -1.0 negative). A p -value of < 0.05 was considered statistically significant with a confidence interval of 95%.

Design of illustrations: Figures showing experimental setup, cellular mechanistic and the graphical abstract were designed with Biorender.com.


3 | RESULTS

3.1 | Proof of concept: Correlation of neutrophil-to-lymphocyte ratio with HNSCC progression

We started our investigation by examining the potential significance of neutrophils (NØ) in the progression of head and neck squamous cell carcinoma (HNSCC). To this end, we assessed the neutrophil-to-lymphocyte ratio (NLR) across different tumour stages in HNSCC patients, employing the staging criteria from the Union for International Cancer Control (UICC). We observed a distribution of NLR values across various disease stages. Our cohort consisted of 76 patients, with a gender distribution of 34.2% females and 65.8% males, with an average age of 67.0 ± 9.4 and 63.6 ± 7.9 years, respectively. The diverse tumour site includes 40.8% in the alveolar ridge, 26.3% in the oral cavity and/or tongue, and 19.7% at the floor of the mouth as the most prevalent locations. The NLR was plotted against disease stages I through IVB, revealing a spread of values at each stage. Data demonstrate a significant increase in NLR in relation to the UICC stage, reaching the highest value in the more aggressive type of tumour. The dot line represents the health threshold (NLR = 2.6 (Hsu et al., 2022)) and it is possible to observe that patients data in the stage I and stage II in majority below the dot line, while the stage III shows a higher range between patients, including more samples over the threshold. Tumours classified as UICC stage IVA/B have an increased NLR before surgery, including all patients above the reference line. A shift in the NLR value along the UICC stages is visible. With this regard, the IVA ratio is almost double the stage I ($p < 0.001$) and stage II ($p < 0.01$). Moreover, the IVB stage follows the trend, while significant difference between stage I ($p < 0.01$) and II ($p < 0.05$). The median NLR appeared to increase with the advancement of the disease stage, suggesting a potential link between elevated NLR and disease progression (Figure 1).

3.2 | Characterization of pro-tumour markers in correlation with HNSCC progression

The following step was to randomly select five distinct primary tumours to further characterize their protein marker expression by western blotting (WB). The markers were divided into functional groups for better visualization (Figure 2a). As HNSCC markers, we chose the epidermal growth factor receptor (EGFR) as a frequently overexpressed receptor targeted for HNC therapy and CD44, a cell adhesion molecule currently discussed as an HNSCC stem cell marker. High expression of vimentin and N-cadherin together with low expression of E-cadherin is associated with epithelial-to-mesenchymal transition (EMT). High expression of vimentin and PD-L1 is correlated with poor prognosis, as is high expression of the transcription factors TWIST, an oncogene, and Snail, a tumour suppressor. The purinergic enzymes CD39 and CD73 are frequently associated with tumour malignancy, and elevated levels of adenosine (ADO) in the TME functions as an immunosuppressive molecule. Likewise, overexpression of the inhibitory immune checkpoint molecules PD-L1 and PD-L2 is associated with immunosuppression. The secretion of VEGF and the expression of its receptor VEGFR2 is indicating the angiogenic potential of the tumour. The data suggest that each of the five selected tumours exhibits unique pathological features, as evidenced by the distinct expression profiles of tumour markers specific to HNSCC. These markers reflect the heterogeneity and the spectrum of oncogenic evolution within head and neck carcinogenesis. For instance, primary tumour (PT) #1 shows minimal or no expression of protein markers related to EMT, immune checkpoint regulation and angiogenesis, indicating a preliminary stage of epithelial cell dedifferentiation. Conversely, PT#3 exhibits high expression of these markers suggesting a more advanced stage of cancer progression. Additionally, this analysis highlights the purinergic enzymes expression CD39 and CD73. They are detectable in all PTs, similar to PD-L1, an important immune checkpoint target in immunotherapy.

Female		Male
34.2%		65.8%
67.0 ± 9.4		63.6 ± 7.9
n = 26		n = 50
Tumor site		
Alveolar ridge		40.8%
Floor of mouth		19.7%
Mandible		1.3%
Oral cavity/tongue		26.3%
Planum buccale		3.9%
Retromolar trigone		8.0%

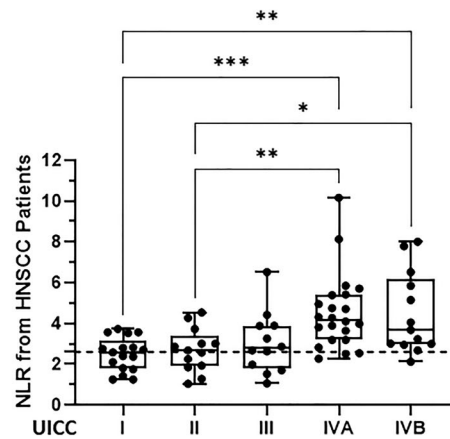


FIGURE 1 Proof of concept: Correlation of NLR with HNSCC progression. This analysis was performed with clinical data from 76 patients with mixed gender. Haemogram was generated pre-operative. Clinical description illustrated as gender percentage, mean of age in years and tumour site. Bar graph depicts the neutrophil-to-lymphocyte ratio (NLR) divided by the UICC staging systems I, II, III, IVA and IVB. The threshold (>2.6) is represented as dot line. The data are presented as mean ± SD, one-way ANOVA with multiple comparison, * $p < 0.05$, ** $p < 0.01$, *** $p < 0.001$. For a more detailed clinical description of the five evaluated HNSCC primary tumours, see Table S1. HNSCC, head and neck squamous cell carcinoma; NLR, neutrophil-to-lymphocyte ratio; UICC, Union for International Cancer Control.

Figure 2b presents the tumour, node, metastasis (TNM) status and patient treatment details for the five HNSCC primary tumour samples selected for this study. It indicates a great variability among the selected samples, which corroborates the characterization panel. The diversity of the five selected primary tumours is reflecting the clinical relevance of cancer pathogenesis and elucidating potential causal relationships for the following observations.

Further, we took a closer look at PD-L1 expression in the tumour samples. Here, we chose a novel approach and investigated the cellular localization of PD-L1 within the cells. Subcellular protein fractionation was performed to separate cells into distinct cellular compartments. Subsequently, the membrane and cytoplasmic protein fractions were analysed for PD-L1 expression (Figure 2c). The subcellular localization of PD-L1 may be indicative of its specific function and localization. Moreover, since EV cargos are prepared in the cytoplasm of the cell, cytoplasmic PD-L1 may also be packed in EVs for subsequent secretion. Interestingly, the ratio of membrane and cytoplasmic PD-L1 expression correlates with the expression pattern of tumour markers. Specifically, PT#1 is characterized by a high PD-L1 membrane expression (mPD-L1) and a lower cytoplasmic PD-L1 (cPD-L1) expression. This observation is in contrast to PT#3, which displays a pronounced cPD-L1 expression with a reduced mPD-L1 expression. The varying ratios of membrane-to-cytoplasmic PD-L1 (mPD-L1/cPD-L1) may indicate differential susceptibilities to immune checkpoint blockade therapies in HNSCC. It is also noteworthy that although PT#5 exhibited the highest overall PD-L1 expression in the characterization panel, the fractionation did not reflect similar expression levels in the membrane and cytoplasmic compartments, indicating a potential nuclear localization that was not investigated in this study.

Considering the pivotal relevance of the subcellular localization of PD-L1 in tumour resistance and progression, we postulated that NLR correlates not only with more aggressive tumour characteristics but also with the intracellular distribution of PD-L1. A Spearman correlation analysis substantiated this hypothesis, revealing a positive correlation between NLR and cPD-L1 ($r = +0.60$) and a negative correlation with mPD-L1 expression ($r = -0.48$). Additionally, the analysis indicated a negative correlation between the mPD-L1/cPD-L1 ratio ($r = -0.54$), as demonstrated in Figure 2d and Table S1.

Currently, only the membrane expression of PD-L1 is relevant for the evaluation in the diagnostic process and the detection of intracellular PD-L1 is neglected. In Figure 2e, we performed an IHC staining the tumour tissue sections with the human anti-PD-L1 antibody clone 28-8, which specifically detects cytoplasmic PD-L1 in addition to membrane-bound PD-L1. PT#1 and PT#3 were selected as representative tumours with lower (PT#1) and higher grade of dedifferentiation (PT#3). In the tissue section of PT#3 a higher percentage of PD-L1 positive cell was detected. Also, a strong cPD-L1 localization is visible in the IHC. Interestingly, PD-L1⁺ tumour cells (here, mPD-L1 and cPD-L1 were counted as PD-L1⁺) correlate with NØ infiltration, indicating a possible synergy of two immunosuppressive mechanisms involved in HNSCC progression. Moreover, we evaluated the central and periphery region of the tumour in relation to CD66b and PD-L1 markers. It is possible to observe a significant positive correlation between these two makers in the central region ($p = 0.0168$), while the periphery follows the same pattern. The total mean of both areas for these markers also correlates ($p = 0.0051$).

These data underscore the integral role of NØ in the context of HNSCC, being potentially influenced by both the malignancy of the tumour and the subcellular localization patterns of PD-L1.

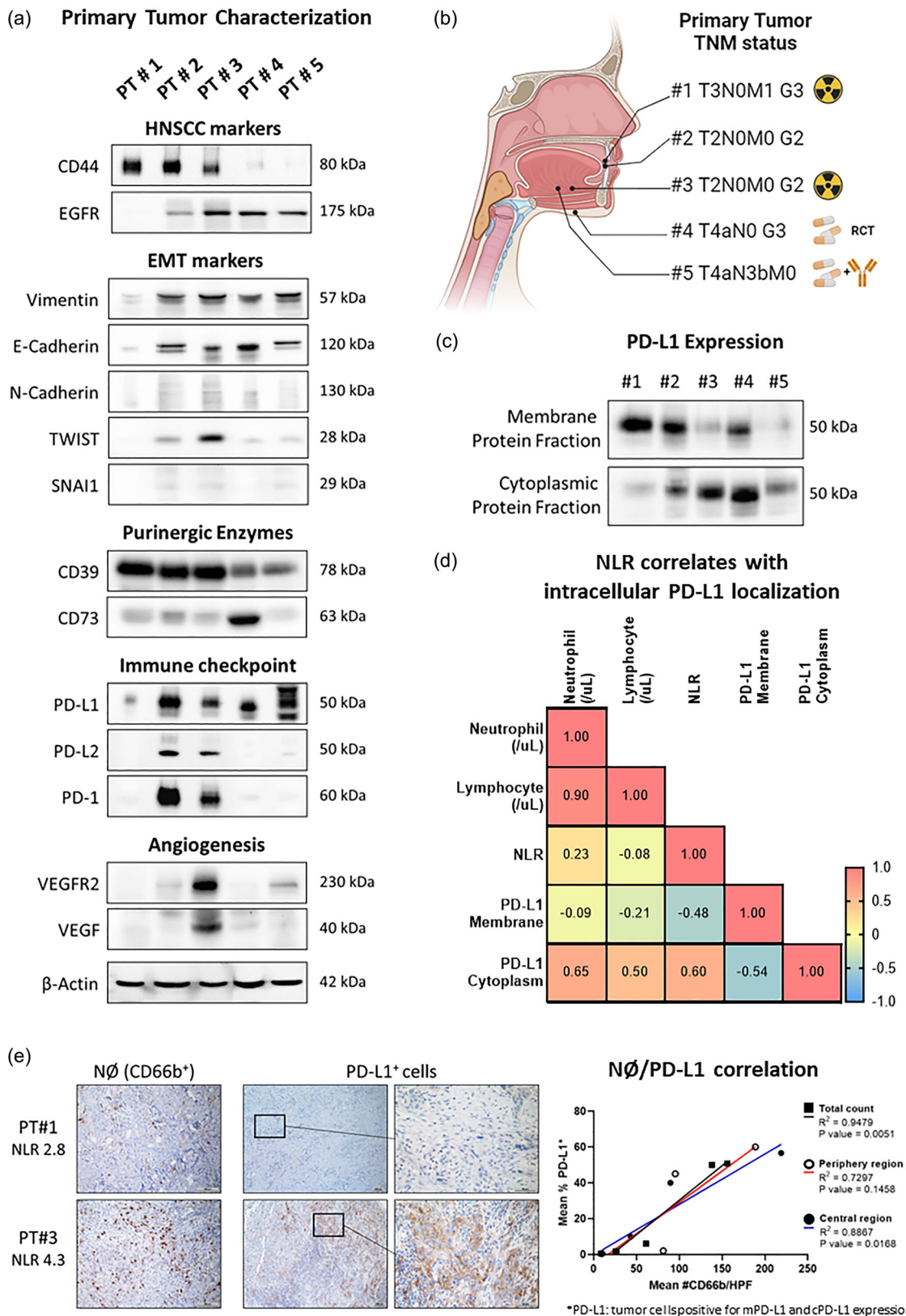


FIGURE 2 NLR correlates with HNSCC progression and intracellular PD-L1 localization. (a) HNSCC primary tumour characterization for PT#1–PT#5 was achieved by western blotting (WB) analysis. Marker expression was divided by HNSCC markers (CD44, EGFR), EMT markers (vimentin, E-cadherin, N-cadherin, TWIST, Snail), purinergic enzymes (CD39, CD73), immune checkpoints (PD-L1, PD-L2, PD-1) and angiogenesis markers (VEGFR2, VEGF). Per sample, 25 μ g of protein was loaded. β -actin was used as loading control. $N = 2$. (b) HNSCC primary tumour TNM status for PT#1–PT#5. The figure indicates the location, staging, and follow-up treatment (radiotherapy, illustrated as trefoil; chemotherapy, illustrated as pill; immunotherapy, illustrated as antibody, RCT = radio-/chemotherapy). (c) WB analysis of PD-L1 expression after subcellular fractionation into membrane and cytoplasmic proteins for PT#1–PT#5. $N = 2$. (d) Heat map of Pearson correlation between NLR and cellular PD-L1 localization for PT#1–PT#5. (e) Immunohistochemical (IHC) stainings of HNSCC

(Continues)

FIGURE 2 (Continued)

primary tumour sections from representative PT#3 for neutrophils (NØ, CD66b⁺) and PD-L1-positive tumour cells (clone 28-8). Correlation of NØ presence and PD-L1⁺ tumour cells was assessed by simple linear regression analysis. R squared and P values were shown for each evaluation: Mean of total PD-L1 percentage, PD-L1 expressed at the periphery and PD-L1 expressed in the central region. PD-L1 staining was magnified for optimized visualization of subcellular PD-L1 localization. Scale bar NØ (CD66b⁺) 100 µm (20x magnification), PD-L1⁺ 100 µm (10-fold magnification) and 50 µm (40-fold magnification). Original blots and additional IHC stainings for characterization of pro-tumour markers in HNSCC primary tumours are shown in Figure S2. For positive cell counts see Table S2. HNSCC, head and neck squamous cell carcinoma; NLR, neutrophil-to-lymphocyte ratio; UICC, Union for International Cancer Control; PT, primary tumour.

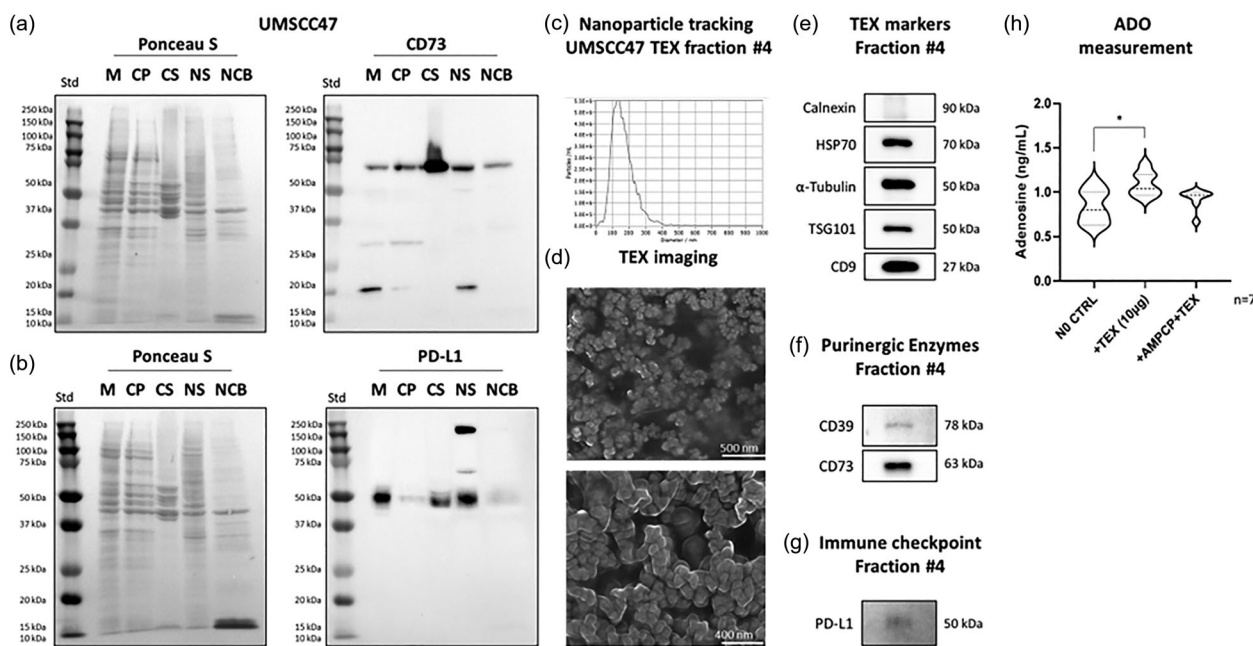


FIGURE 3 Immunosuppressive TEX carry PD-L1 and adenosine producing enzymes. Immunodetection of CD73 (a) and PD-L1 (b) by WB after subcellular fractionation. Subcellular fractions were divided into M, CP, CS, NS and NCB protein fraction. Molecular marker is indicated as Std, ranging from 10 to 250 kilodalton (kDa). Per sample, 20 µg of protein was loaded. Equal loading is verified by Ponceau S staining. $N = 2$. (c) Results of nanoparticle tracking analysis of fraction #4 from HNSCC cell line SCC47. Scale bars, 400/500 nm. (d) Scanning electron microscopic (SEM) image of fraction #4. $N = 2$. (e) Representative WB of fraction #4 using the TEX markers Calnexin, HSP70, α -Tubulin, TSG101 and CD9. (f) Immunodetection of purinergic enzymes CD39 and CD73. $N = 2$. (g) Immunodetection of immune checkpoint PD-L1. $N = 2$. For WB analysis, 10 µg of protein lysate was used. (h) ELISA analysis of extracellular adenosine in the supernatant of experimental groups. Cells incubated with the respective cell culture medium served as experimental control. Non-conditioned media was used for background signal subtraction. The data are presented as mean \pm SD ($n = 7$). * $p < 0.05$ versus control group. Original blots for SCC47-TEX characterization are shown in Figure S3. CP, cytoplasmic; CS, cytoskeletal; HNSCC, head and neck squamous cell carcinoma; M, membrane; NCB, nuclear chromatin-bound; NS, nuclear soluble; WB, western blotting.

3.3 | Immunosuppressive TEX carry PD-L1 and adenosine producing enzymes

HNSCC mediates immunosuppressive effects both locally within the TME and systemically. Investigating the potential of TEX to facilitate this immunosuppression we used the HNC cell line SCC47, known for its capacity of secreting high amounts of sEVs. Subcellular protein fractionation of these cells revealed a distribution of the CD73 enzyme, with a molecular weight of approximately 70 kDa across all fractions, with higher expression in the cytoskeletal fraction (Figure 3a). Interestingly, the subcellular fractionation also revealed the presence CD73 with a lower molecular weight of approximately 21 and 28 kDa. To the same extent, PD-L1 was predominantly detected at the cellular membrane, cytoskeleton, and nuclear soluble protein fraction, including PD-L1 variants around 70 and >150 kDa (Figure 3b).

Subsequent TEX isolation using mini-SEC method yielded a population of particles isolated from fraction #4 with a size of 100–150 nm, confirmed by SEM to be vesicular aggregates (Figure 3c,d). WB analysis confirmed the presence of positive markers for CD9, TSG101, α -Tubulin, HSP70 in the absence of Calnexin (Figure 3e). These results confirm that fraction #4 contained isolated SCC47 TEX.

Interestingly, Figure 3f demonstrated that TEX carried the markers CD39 and CD73, indicating potential purinergic enzyme activity. They also exhibited PD-L1 expression (Figure 3g).

Quantification of adenosine (ADO) in the supernatant of TEX-treated cultures indicated an increase in ADO production in the TEX-NØ mixed culture, which persisted albeit at a reduced level when the CD73 enzyme was pharmacologically inhibited

with AMPCP, ($p < 0.05$, Figure 3h), but still remained higher than in the control group without TEX treatment (NØ CTRL). The presented evidence suggests that TEX carry purinergic enzymes and can be a source of extracellular ADO. Altogether, data show that both immunosuppressive proteins, PD-L1 and CD73, can be found in the intracellular compartment, which can indicate their presence as cargo in EVs. After isolating and characterizing SCC47-derived TEX, both purinergic and PD-L1 immunodetection were positive and a source of ADO.

3.4 | TEX–neutrophil crosstalk

To investigate the chemoattractive properties of TEX on NØ, we conducted a transwell migration assay (Figure 4a). The number of NØ in the lower chamber was normalized using the positive control (CTRL) to exclude individual reactivity variables. In Figure 4b, we observed a significant migration of NØ cells toward TEX ($p < 0.05$). This chemotactic response was attenuated by ADO signalling, as shown by reduced migration of NØ after blockade of the adenosine receptor P1R with CGS15943 and inhibition of CD73 with AMPCP ($p < 0.001$; $p < 0.0001$), suggesting that TEX-induced chemotaxis is modest but dependent on ADO signalling.

To further explore the interaction of TEX with NØ, we performed SEM imaging. Notably, SEM imaging revealed NØ surfaces bound with TEX, whereas CTRL NØ demonstrated a smooth surface (Figure 4c). Immunofluorescence staining also revealed the retention of TEX (green) on the NØ confirming the physical association between TEX and NØ. The ADO signalling impairment does not influence the TEX–NØ interaction, as shown in Figure 4d.

Overall, the data suggest that TEX not only serve as chemoattractant to NØ but also maintain sustained interaction, highlighting a potential mechanism for TEX-mediated modulation of the NØ response. Blocking P1R and CD73 reduced NØ migration.

3.5 | Characterization of TEX-modulated neutrophils phenotype

Our analysis investigated how TEX influence the phenotype of NØ and whether they shift them to an anti- or pro-tumour state. Therefore, we selected CD11b⁺/CD66b⁺ cells that were classified into two distinct subsets, based on the expression levels of CD170. These subsets are referred to as “CD170^{low}” and “CD170^{high}” population. A representative gating strategy is shown in Figure 5a. The combination of the analysed marker expression CD11b⁺/CD66b⁺/CD170⁺ to define anti- and pro-tumour NØ subpopulations is supported by previous findings of Jaillon et al. (2020).

In general, we observed that the interaction of NØ with TEX (+TEX) led to a significant increase in a CD170^{high} pro-tumour population compared to the control group NØ w/o TEX (CTRL) ($p < 0.0001$ –Figure 5b). Additionally, the ratio of CD170^{high} to CD170^{low} cells doubled following TEX treatment ($p < 0.001$). Regardless of the increase of the CD170^{high} population, both subpopulations are present across all groups. Despite a predominant CD170^{low} population in the CTRL group ($p < 0.05$), the addition of TEX consistently resulted in a higher proportion of CD170^{high} cells. To determine the role of ADO signalling in NØ phenotypes, we blocked the adenosine receptor P1R and assessed CD170 positive subpopulations. Notably, blocking A2_B receptor (MRS1754) led to a noticeable increase in the CD170^{high} subpopulation in comparison to the control (NØ CTRL, $p < 0.05$), suggesting a potential link between ADO signalling and NØ phenotype polarization.

In Figure 5c, the correlation between CD73 expression with regards to the activation of anti-/pro-tumour NØ was explored. TEX-modulated NØ showed a similar pattern in CD73 expression. The CD170^{high} subpopulation exhibited higher CD73 expression, while the CD170^{low} subpopulation demonstrated lower expression. Notably, when comparing to CD170^{low} subpopulation in TEX group, there was more than a significant two-fold increase in CD73 MFI ($p < 0.005$). This increase also stood out in comparison to the CTRL group, where the CD170^{high} subpopulation displayed double the CD73 intensity ($p < 0.005$). Treatment with the A3 receptor (A3R) antagonist PSB10 resulted in a decrease in CD73 expression, bringing the pro-tumour subgroup closer to control levels, indicating the role of ADO signalling in modulating the phenotype. Interestingly, when blocking A3R, the subpopulation distribution in this group is similar to the CTRL, which indicates a possible reverse activation.

Furthermore, western blot analysis in Figure 5d revealed that TEX treatment upregulates the immune checkpoint protein PD-L1 in NØ ($p < 0.05$). PD-L1 expression is, another marker associated with pro-tumour NØ. Interestingly, blocking A2_BR exhibited a synergistic effect, further increasing PD-L1 protein expression compared to CTRL ($p < 0.005$) and TEX-modulated groups ($p < 0.05$). On the other hand, blocking A3R inhibited TEX modulation of PD-L1 expression ($p < 0.05$). Since the TEX incubation in each group is consistent, the variance of immunodetection in response to different treatments points out that PD-L1–TEX are not interfering in the PD-L1 NØ expression.

To investigate the impact of TEX on the secretome of NØ, we employed a Human Cytokine Array to detect multiple cytokines, chemokines, growth factors and other soluble proteins in cell culture supernatant of the NØ (Figure S4a). Analysis indicated that TEX treatment led to a notable upregulation of two cytokines in the NØ secretome, as shown in Figure 5e: CCL1/I-309 and Serpin E1/PAI-1 saw increases of 1.5-fold ($p < 0.05$) and >1.5-fold ($p < 0.0001$), respectively, compared to the control. However,

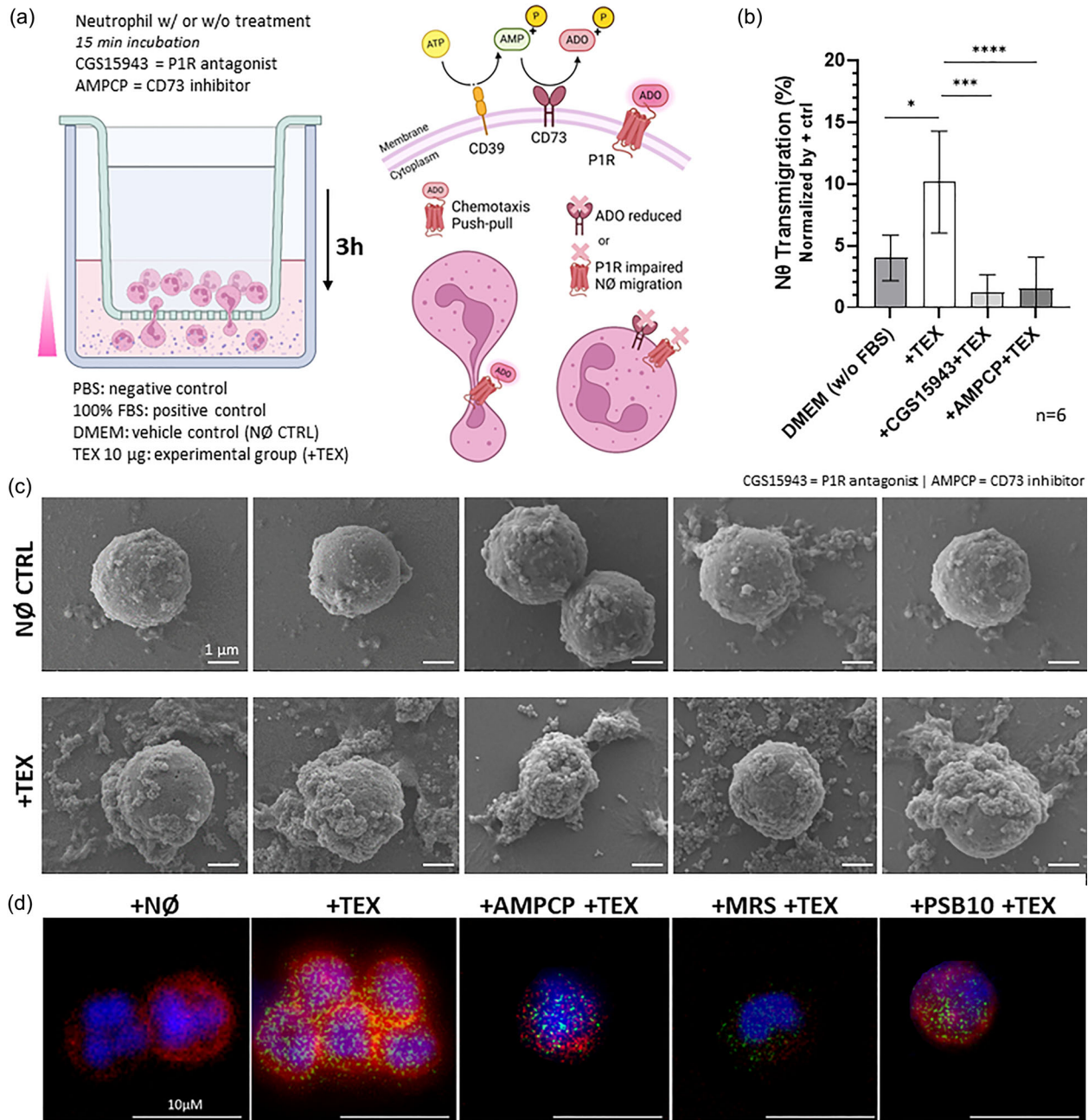
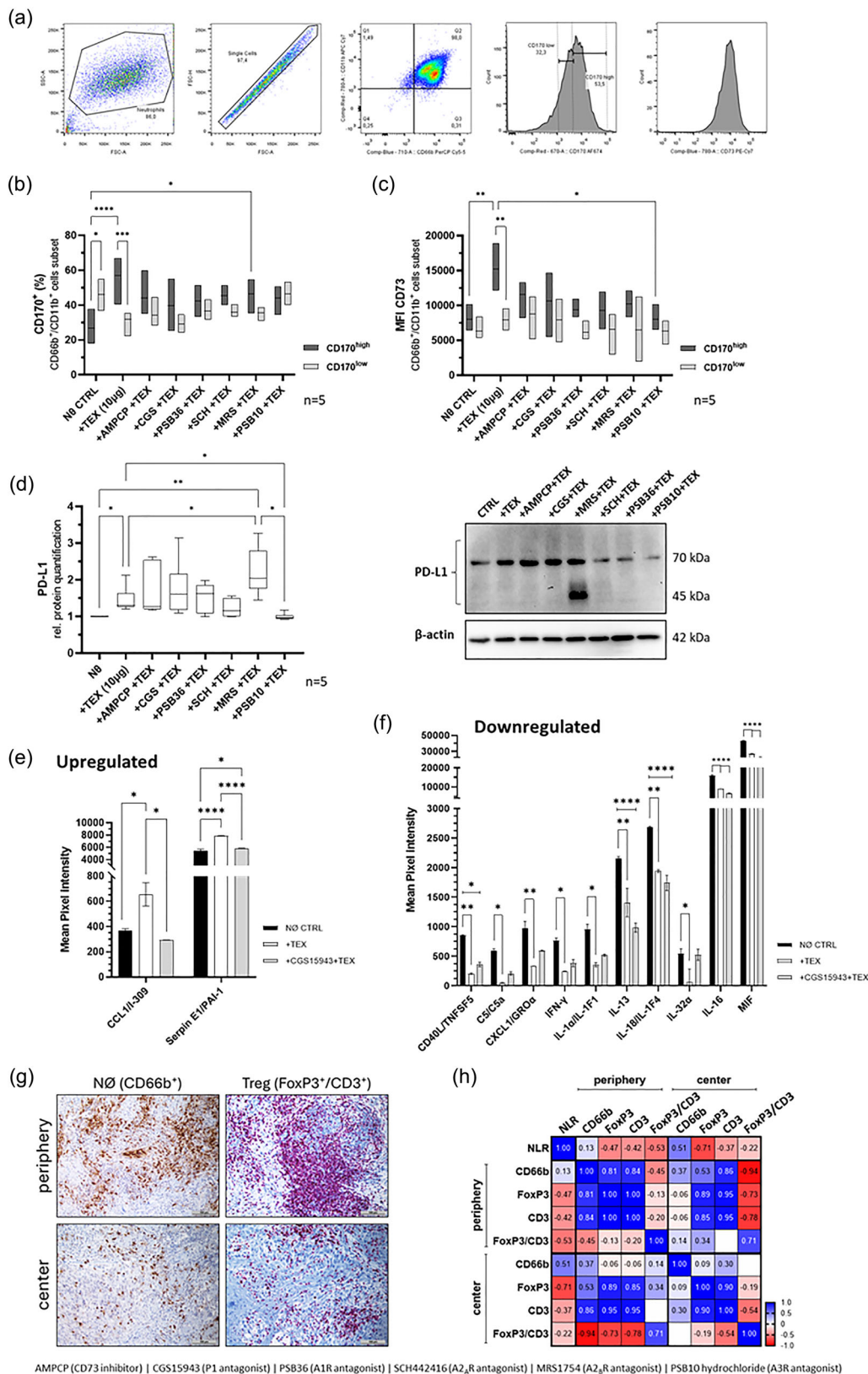


FIGURE 4 TEX–neutrophil crosstalk. (a) Representation of the transmigration assay experimental design and a schematic overview of the neutrophil (NØ) response to ADO signalling inhibition. The upper chamber contains NØ with (w/) or without (w/o) pre-incubation with the P1R antagonist CGS15493 or the CD73 inhibitor AMPCP. The lower chamber contains the following chemoattractants: PBS for negative chemotaxis control; 100% FBS as positive chemotaxis control; DMEM w/ 10% EDHI FBS, as vehicle/NØ control; and DMEM w/ 10% EDHI FBS +TEX as experimental group. Cells are defined as migrated due to their presence in the bottom chamber after 3 h of incubation in the experimental transwell setup. (b) Normalized percentage of NØ migration through the permeable membrane pores into the bottom chamber ($n = 6$ per group). Control group was composed by NØ exposed to non-conditioned medium, which was prepared as described in the material and methods section. Graph show mean \pm SD and significance values were calculated using multiple one-way ANOVA * $p < 0.05$, **** $p < 0.0001$. (c) Selection of five representative SEM images from NØ CTRL versus NØ interacting with TEX (+TEX). Scale bar = 1 µm ($n = 15$). (d) One representative immunofluorescence image with DAPI = blue, phalloidin = red, TEX = green per group. Scale bar = 10 µm ($n = 15$ per group). NØ CTRL, NØ control group.

this upregulation was attenuated when P1R was blocked in NØ by CGS15943, causing the levels of these cytokines to return to baseline. Conversely, TEX treatment induced a significant downregulation of 10 cytokines (Figure 5f). Interestingly, blocking P1R (CGS15943) did not restore the secretion levels of these cytokines to normal, suggesting that the impact of TEX on their secretion was independent of P1R signalling.



AMPCP (CD73 inhibitor) | CGS15943 (P1 antagonist) | PSB36 (A1R antagonist) | SCH442416 (A2,R antagonist) | MRS1754 (A2,R antagonist) | PSB10 hydrochloride (A3R antagonist)

FIGURE 5 Characterization of TEX-modulated Neutrophils phenotype. (a) Representative gating strategy for the detection of CD170^{high} or CD170^{low} subpopulations among NØ. Selection of SSC versus FSC NØ population follows exclusion of doublets, using FSC-H versus FSC-A, followed by the selection of CD66b⁺/CD11b⁺ population. Histograms represent the final strategy to select CD170^{low} and CD170^{high} populations and the MFI for CD73. (b) Identification of the anti/pro-tumour phenotype, based on the CD170^{low} and CD170^{high}, respectively. Plots are shown for gated live CD66b⁺ CD11b⁺ cells w/ or w/o ADO signalling blockade. (c) MFI detection of CD73 cells from gated CD170^{high} or CD170^{low}. (d) Immunodetection of PD-L1 in NØ. In this representative blot, 25 µg of protein lysate was loaded onto a 10% acrylamide gel. β-actin was used as loading control. Results are shown as fold change relative to control group (NØ) (n = 5 per group). (e), (f) Human cytokine array was used on pool supernatant from five pooled donors per group: non-treated NØ as control (CTRL),

(Continues)

FIGURE 5 (Continued)

NØ cultured with TEX (+TEX) and NØ pre-treated with PIR antagonist CGS15943 and subsequently cultured with TEX (+CGS +TEX) for 48 h. Pixel intensity analysis of the dots from the membranes was performed to determine the relative expression levels of inflammatory cytokines. Results are representative of a pool of five donors in each group. Bars represent pixel intensity analysis of the dots. (e) Upregulated cytokine secretion and (f) downregulated cytokine secretion. Graphs show mean \pm SD and significance values were calculated using multiple 2-way ANOVA. * $p < 0.05$, ** $p < 0.01$, **** $p < 0.0001$. Control group was composed by NØ exposed to non-conditioned medium, which was prepared as described in the material and methods section. (g) Representative IHC images from PT#3 for CD66b⁺, CD3⁺ and FoxP3⁺. Scale bar 100 μ m (20-fold magnification). (h) Pearson Correlation matrix of IHC analysis for the presented markers CD66b, CD3 and FoxP3 at the periphery and central regions. Positive correlation is highlighted in blue, negative correlation in red. Original dot blots of Human Cytokine Array and additional IHC stainings for correlation of NØ presence with Treg infiltration in HNSCC primary tumours are shown in Figure S4. For positive cell counts see Table S2.

The IHC analysis of the five above mention patients revealed that NØ infiltration in the tumour periphery can modulate the lymphocyte profile in both tumour periphery and tumour centre (Figure 5g). The correlation matrix indicates that in the tumour periphery, the presence of NØ (CD66b⁺) positively correlates with Treg (FoxP3⁺) and CD3⁺ cell counts. Similarly, CD3⁺ cells in the tumour periphery predominantly consist of Tregs. These findings highlight a significant influence of NØ on the infiltration of Tregs (Figure 5h).

Interestingly, the immune profile in the tumour centre is greatly influenced by peritumoral infiltration. The graph illustrates that increasing levels of peritumoral CD66b⁺ and FoxP3⁺ cells also increase the presence of both CD3⁺ and FoxP3⁺ cells in the central area. Furthermore, the FoxP3 marker negatively correlates with the NLR, indicating that higher levels of circulating NØ result in fewer lymphocytes infiltrating the tumour. This trend is also observed in the ratio of FoxP3⁺ to CD3⁺ cells, where a higher ratio suggests an increased presence of Tregs. The data demonstrates that the FoxP3/CD3 ratio in the tumour centre decreases with increased NØ infiltration in the periphery. Overall, this dataset illustrates a close relationship between NØ and lymphocyte profile infiltration, suggesting that NØ play a role in recruiting more Tregs.

These findings highlight the potential role of TEX in modulating the phenotype of NØ and suggest their involvement in the regulation of pro-tumour responses by selectively modulating the cytokine profile of NØ. Moreover, their effects on cytokine secretion may involve mechanisms beyond PIR activation.

3.6 | The dynamic modulation of CD73/PD-L1 axis by pro-tumour neutrophils

The previous observations raised the question of whether this acquired pro-tumour NØ phenotype could actually promote tumour progression. Therefore, SCC47-derived TEX were incubated with primary NØ, pre-treated with antagonist according to experimental group (+AMPCP+TEX; +MRS+TEX; +PSB10+TEX), for 24 h. Next, the primed TEX-modulated NØ were cultured with four different HNC cell lines: SCC47, SCC9, PCI52 and FaDu, for 48 h, as explained in the graphical experimental design (Figure 6a). Since PD-L1 modulation in tumour cells is an interesting target of this study, we evaluated the PD-L1 expression in each cell line, along with the CD73 and CDK6 modulation. Representative WB results after co-cultivation of tumour spheroids from SCC47 with NØ are shown in Figure 6b and Figure S5 for SCC47, SCC9, PCI52 and FaDu. The semiquantitative WB analysis of all cell lines in Figure 6c shows significant influence of NØ incubation with the HNC cell lines. The expression of PD-L1 (0.17 ± 0.11 ; $p < 0.0001$) and CDK6 (0.35 ± 0.20 ; $p < 0.001$) is significantly downregulated in all cell lines, CD73 expression shows the same trend (0.35 ± 0.33 $p = 0.361$). Interestingly, co-cultivation with TEX-modulated NØ (+TEX) leads to an upregulation PD-L1 and CD73 expression across all cell lines, in comparison to the NØ control without TEX-modulation (+NØ). Moreover, inhibition of CD73 (+AMPCP+TEX) resulted in downregulation of PD-L1 in tumour cells, while blocking the adenosine receptor A2_B with MRS1754 (+MRS+TEX) notably enhanced PD-L1 expression in comparison to +TEX. Blocking A3 receptor (+PSB10+TEX) showed no modulation on PD-L1 but a slight increase in CD73 expression, in comparison to the +TEX group. Altogether, the quantitative analysis demonstrated a pattern of reduced PD-L1 and CD73 in tumour spheroids cultured with unmodified NØ (+NØ). Interesting to notice is a slight but significant increase of expression in these proteins when tumours were cultured with TEX-primed NØ (+TEX). As observed previously with NØ pro-tumour phenotype, blocking A2_B in NØ synergized with TEX to promote tumour progression, by increasing both PD-L1 and CD73 proteins. Conversely, inhibiting CD73 activity (+AMPCP+TEX) or blocking A3R (+PSB10+TEX) attenuate the pro-tumour actions of NØ as demonstrated by the decrease in the CD73/PD-L1 axis. The figure also illustrates that the dynamic expression of the CD73/PD-L1 axis is linked to the inhibition of CDK4/6 signalling.

To validate the before mentioned data, an *in ovo/ex vivo* culture was performed with primary tumours (PT) from HNSCC patients (HPV^{neg}, low PD-L1 combined positive score (CPS = 25%)) (Figure 6d,e). The tumours were treated with NØ-derived secretomes treated with SCC47-derived TEX. The results indicate an increase in PD-L1 and CD73, and a decrease in CDK6 and Cyclin D1 expression in tumours treated with TEX-modulated NØ secretome. Interestingly, healthy NØ secretome (PT+NØ) presented a slight decrease in PD-L1, and an increase in Cyclin D1, suggesting PD-L1 degradation via the Cyclin D-CDK4/6 pathway. Notably, the +TEX group and +CGS+TEX depict opposite responses. While +TEX treatment increased CD73 together

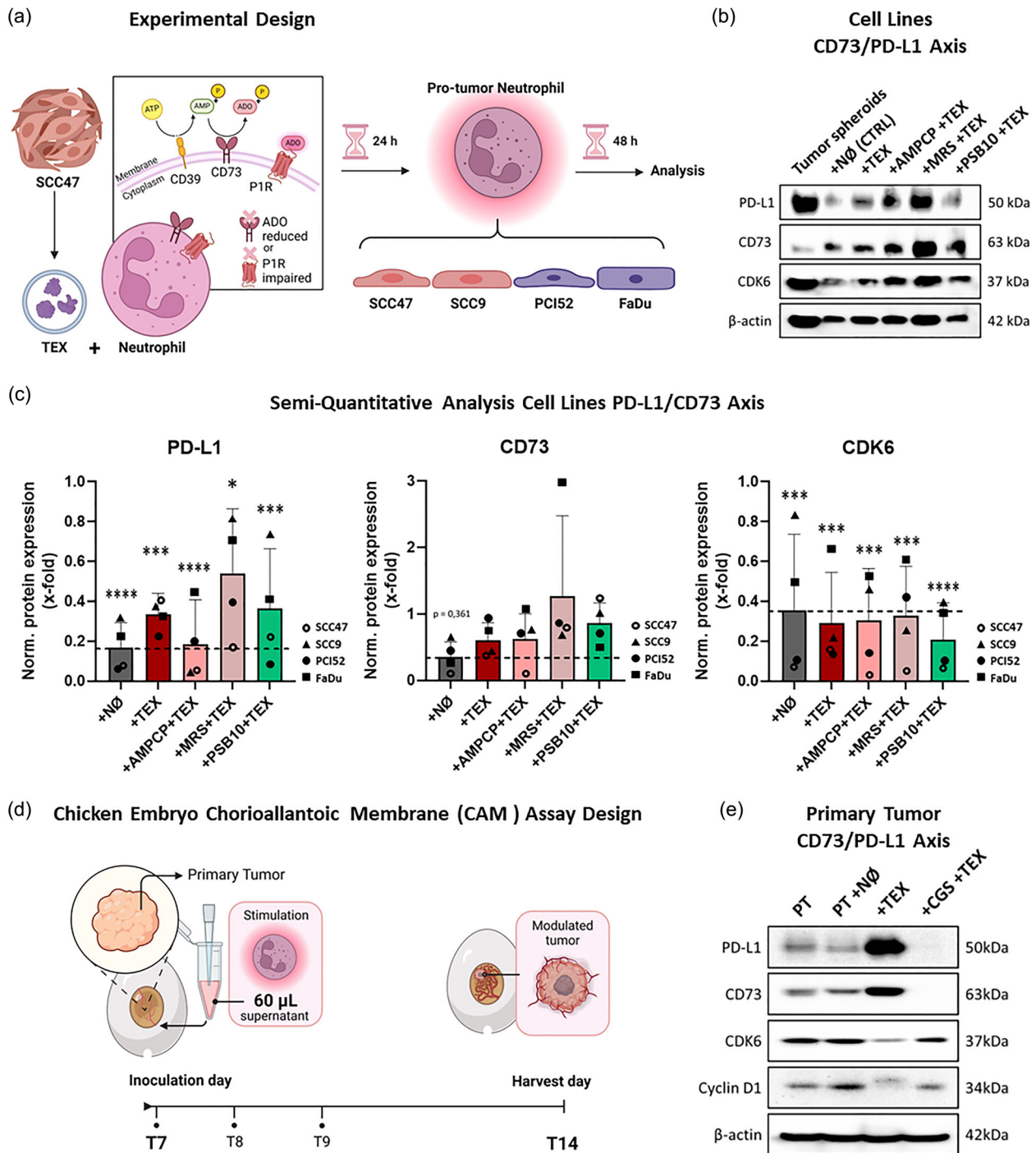


FIGURE 6 The dynamic modulation of CD73/PD-L1 axis by pro-tumour neutrophils. (a) Experimental design of the *in vitro* modulation in HNC cell lines SCC47, SCC9, PCI52 and FaDu. (b) Immunodetection of PD-L1, CD73 and CDK6 after treatment with Neutrophils (+NØ), NØ with 10 µg of TEX (+TEX), NØ pre-treated with CD73 inhibitor followed by TEX incubation (+AMPCP +TEX), NØ pre-treated with A2 β R antagonist MRS1754 followed by TEX incubation (+MRS +TEX), NØ pre-treated with A3R antagonist followed by TEX incubation (+PSB10 +TEX) compared to control (HNC cell line = CTRL). Prior to lysis, NØ were washed out to reduce NØ interference in the measurement. Per sample, 10 µg of protein was loaded. β -actin was used as loading control. HNC cell line PCI52 was used as a representative. Additional cell lines FaDu, SCC9 and SCC47 are shown in Figure S5. $N = 3$. (c) Semi-quantitative analysis of western blots. Protein expression was normalized to the loading control β -actin. Graphs show mean \pm SD and significance values were calculated using multiple two-way ANOVA. * $p < 0.05$, *** $p < 0.001$, **** $p < 0.0001$. (d) Illustration of the chicken embryo chorioallantoic membrane (CAM) assay design. (e) Immunodetection of PD-L1, CD73, CDK6 and Cyclin D1 after 7-day CAM protocol. Groups divided as treatment of HNSCC primary tumour with healthy neutrophil supernatant (PT +NØ), NØ with TEX (+TEX), or NØ pre-treated with P1R antagonist followed by TEX incubation (+CGS +TEX) compared to control (HNSCC primary tumour = PT). Per sample, 25 µg of protein was loaded. β -actin was used as loading control. $N = 3$. Original blots are shown in Figure S6.

with PD-L1 while Cyclin D1/CDK6 levels were decreased. The addition of CGS15943 (PI3R antagonist) prior to TEX exposure reversed this effect, lowering the immunosuppressive axis and suggesting a more favourable tumour response (Figure 6e).

3.7 | Endorsement of pro-tumour potential of TEX-modulated neutrophils

The pro-tumour effects of the TEX-modulated NØ were also evaluated by functional assays with four different HNC cell lines: SCC47, SCC9, PCI52 and FaDu. Figure 7a illustrates a representative result of the proliferation rate of cell line SCC47. The significances between the groups corroborates with the previous pattern described for CD73/PD-L1 axis expression. We observed a notable increase in the proliferation of SCC47 cells, when cultured with pro-tumour NØ, compared to healthy NØ. A similar result was observed in HNC cell line SCC9 ($p < 0.05$; Figure S7). Interestingly, the group treated with the A_{2B}R antagonist MRS1754 (+MRS+TEX) displayed even higher proliferation rates ($p < 0.01$), while the group with A3 receptor blockade (+PSB10+TEX) showed a decrease in proliferation. Conversely, PCI52 and FaDu demonstrated reduced proliferation with TEX treatment compared to controls ($p < 0.0001$ and $p < 0.001$, respectively). Caspase 3/7 assays were utilized to determine the rate of cell death in each cell line, which endorsed the proliferation findings (Figure 7b).

To understand the direct effects of pro-tumour NØ on tumour cells, we performed a cell spreading and wound healing (scratch) assay. Area quantification between 2 h and 48 h shows a similar pattern as mentioned before for HNC cell line SCC47. An increase in cell spreading when incubated with TEX-modulated NØ ($p < 0.01$), a tumour regression in the spheroids incubated with NØ+AMPCP+TEX ($p < 0.001$) and +PSB10+TEX ($p < 0.0001$) groups, and a slightly reduction in boosting tumour spreading when NØ were treated with A_{2B}R blocking before TEX interaction ($p < 0.05$; Figure 7c) could be observed. HNC cell line SCC9 and FaDu did not presented significant differences between healthy NØ (+NØ) and pro-tumour NØ (+TEX). Besides, FaDu seems to not be affected by the TEX-NØ modulation. Representative figures from the SCC47 cell spreading are shown in Figure 7d.

Next, the scratch assay was performed with HNC cell line SCC47 (Figure 7e) and SCC9. Data further confirmed that TEX-modulated NØ accelerate wound healing in SCC47, with significant differences from the CTRL within 5 h ($p < 0.01$) and 10 h ($p < 0.05$). With regards to ADO antagonists, blocking A3R on NØ alters their effects as shown before and slows down the healing rates ($p < 0.05$). The same late healing pattern with +PSB+TEX group could be observed in cell line SCC9 within 10 h ($p < 0.0001$; Figure S7d). Lastly, these results corroborate with the proliferation assay in all four cell lines (Figure S7). To comprehend the diverse responses of cell lines to TEX-mediated NØ interaction, we conducted a cell line characterization. SCC47 and SCC9 exhibit comparable marker expression, except for CD73, which is more elevated in SCC9. In contrast, PCI52 demonstrates a distinct mesenchymal phenotype, while FaDu falls between these observations (Figure S8).

Taken together, the presented data suggest that pro-tumour NØ can enhance tumour progression, with variable effects across different cell lines. The interaction between tumour cells and pro-tumour NØ also appears to boost PD-L1 expression, highlighting the influence of NØ phenotype on tumour PD-L1 levels.

4 | DISCUSSION

4.1 | NLR and PD-L1 dynamics in carcinogenesis

The neutrophil-to-lymphocyte ratio (NLR) serves as a recognized inflammatory biomarker, reflecting the balance between neutrophil and lymphocyte counts (Masucci et al., 1146). Elevated NLR is linked to poor prognosis in various cancers. In HNSCC, NLR is under investigation for its diagnostic, prognostic, and predictive potential (Mascarella et al., 2018; Takenaka et al., 2022). Our study extends this by exploring correlations between NLR and key tumorigenic processes across five primary tumours from distinct head and neck locations, also representing different stages of tumour development. This comprehensive assessment emphasizes the nuanced associations of the identified biomarker with HNSCC progression.

We focused on investigating PD-L1 expression and its cellular localization, recognizing its role in both immunosuppression and cell-intrinsic functions in tumour cells (Boussiotis, 2016; Chen et al., 2017; Gato-Cañas et al., 2017; Mortezaee, 2020). Our previous studies highlighted PD-L1's influence on cell cycle progression, proliferation, motility, invasion, and survival after irradiation (Eichberger et al., 2020; Schulz et al., 2019; Schulz et al., 2021). PD-L1 expression varies with cell differentiation status, with mesenchymal cells showing higher levels than epithelial cells. Clinically used treatments alter PD-L1 localization, observed differently in highly malignant tumours. In the five tumours under investigation, we observed variations in the subcellular localization of PD-L1, specifically between the cell membrane and cytoplasm. Currently, only membrane expression of PD-L1 is relevant for clinical PD-L1 scoring by IHC. The presence of intracellular PD-L1 is entirely neglected and in most cases is not even detectable with the diagnostic anti-PD-L1 antibodies used. This might explain for the low predictive value of PD-L1 positivity for immune checkpoint inhibition. Figure S9 provides a comparison of three human anti-PD-L1 antibody clones available for diagnostics: 22C3, EIL3N and 28-8. On serial HNSCC tissue sections they differ significantly in PD-L1 detection potential. While 22C3 has

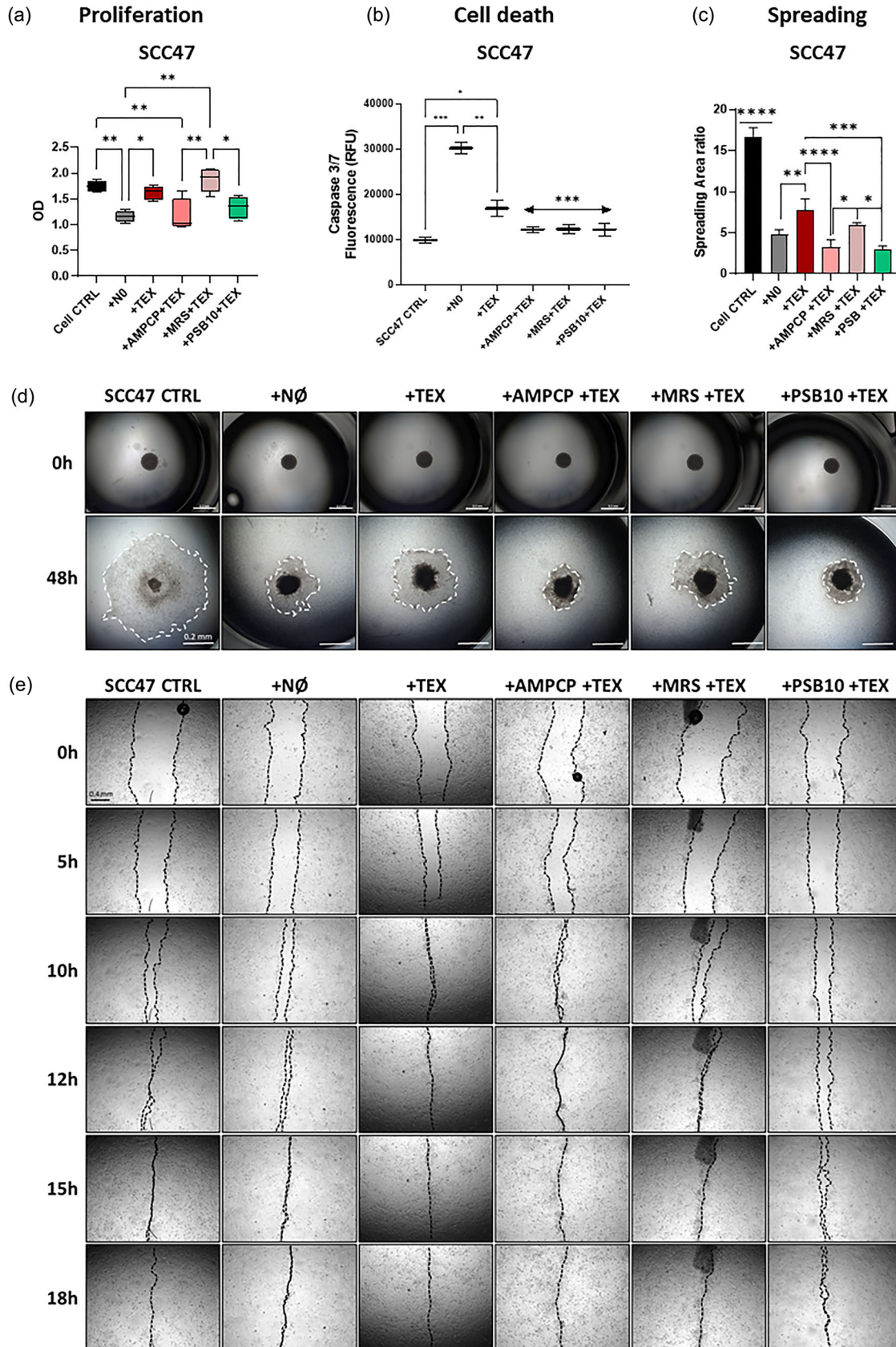


FIGURE 7 Endorsement of pro-tumour potential of TEX-modulated Neutrophils. Functional assays were performed with HNC cell lines SCC47, SCC9, PCI52 and FaDu with the following treatment groups: control (HNC cell line = CTRL), tumour cells with Neutrophils (+NØ), tumour cells with NØ with 10 µg TEX (+TEX), tumour cells with NØ pre-treated with CD73 inhibitor followed by TEX incubation (+AMPCP +TEX), tumour cells with NØ pre-treated with A_{2b}R antagonist MRS1754 followed by TEX incubation (+MRS +TEX) and tumour cells with NØ pre-treated with A_{3R} antagonist followed by TEX incubation (+PSB10 +TEX) indicated by distinct symbols and colours. (a) Quantitative analysis of cell proliferation assay by MTS absorbance (OD) with the

(Continues)

FIGURE 7 (Continued)

representative HNSCC cell line SCC47. $N = 5$. Cell lines SCC9, PCI52 and FaDu are shown in Figure S7. (b) Quantitative analysis of cell death assay by caspase 3/7 fluorescence as relative fluorescence units (RFU) with the representative HNSCC cell line SCC47. $N = 3$. (c) Quantitative analysis of spreading assay by area ratio (area 48 h after incubation divided by area right before treatment) with the representative HNSCC cell line SCC47. $N = 3$. (d) One representative image of spreading assay per group at the beginning of the experiment (0 h) and after 48 h of incubation (48 h), performed with representative HNSCC cell line SCC47. Spreading area is highlighted with a dot line. Scale bar = 0.2 mm. $N = 3$. (e) Representative images of wound healing assay 0, 5, 10, 12, 15 and 18 h after treatment, performed with SCC47. Scratch is highlighted with a dot line. Scale bar = 0.4 mm. $N = 3$. Graphs express mean \pm SD and significance values were calculated using multiple 2-way ANOVA. * $p < 0.05$, ** $p < 0.01$, *** $p < 0.001$. For proper comparison, cells from all groups were incubated in the same cell culture media condition. HNSCC, head and neck squamous cell carcinoma.

the lowest detection capacity, EIL3N and 28-8 detect both, membrane-bound and intracellular PD-L1. Since the highly specific clone 28-8 yielded the strongest mPD-L1 and cPD-L1 detection in this comparison, we decided to perform IHC staining in Figure 2e with clone 28-8. Notably, the localization tends to differ in relation to the tumour's aggressiveness, with a more internal localization observed in highly malignant tumours (Schulz et al., 2024). This intriguing finding prompted an investigation into the potential correlation between the subcellular localization of PD-L1 and the NLR. Notably, there is a robust positive correlation between NLR values and the expression of PD-L1 in the cytoplasm of tumours. This is supported by IHC data where it shows a positive correlation between CD66b⁺ and PD-L1 markers. This observation suggests a heightened level of crosstalk and interdependence between tumour cells and NØ within the TME.

4.2 | Pro-tumour neutrophil phenotype is induced by HNSCC-derived TEX

The orchestrated immunosuppression resulting from the concurrent upregulation of CD73 and PD-L1 in the TME has encouraged discussions regarding the mechanisms underlying tumour-immune cross-modulation. In our investigation, subcellular protein fractionation of SCC47 unveiled the presence of PD-L1 in diverse cellular compartments, including the nucleus. Notably, PD-L1 was identified not only in its well-documented glycosylated/deglycosylated states (40–55 kDa) but also in a novel nuclear PD-L1 variant, exhibiting a higher molecular weight of approximately 70 kDa and >150 kDa, as recently reported by Schulz et al. (2024). These findings were similarly observed in six thoroughly characterized HNC cell lines, including SCC9, FaDu, and PCI52. Furthermore, CD73 demonstrated a ubiquitous presence across all subcellular fractions, with particularly pronounced expression in the cytoskeleton, with pro-tumour activity associated with its nucleotidase function. This substantiates the notion that the dynamic trafficking of both proteins may be linked to their release with sEVs, since their high protein expression in the cytoplasm and cytoskeleton may be linked to TEX packing in MVBs and further release (Tang et al., 2020). It has been noted in the literature that sEVs are proficient in generating ADO and may indeed encapsulate ADO within their luminal space. The ADO content within TEX has been specifically associated with their immunosuppressive effects (Ludwig et al., 2020). TEX have been shown to carry various bioactive molecules which can be transferred to recipient cells and modulate their behaviour and functions (Minciacchi et al., 2015). We found that SCC47-derived TEX carry CD73 and PD-L1, immunosuppressive markers that have prognostic value, especially exosomal PD-L1 (Daassi et al., 2020; Niu et al., 2022). Exosomes originating from various cancer types exhibit significant expression of CD73, showcasing a robust ability to generate ADO (Clayton et al., 1950). With this regard, sEVs from HNSCC cell lines were reported to carry the enzyme CD73 (Lu et al., 2022). Besides, TEX derived from SCC47 cells were already reported to not only produce ADO through CD73 enzymatic breakdown, but also carries ADO internally (Ludwig et al., 2020). In addition, quantities of PD-L1 found on TEX are associated with the advancement of HNSCC. Recent findings also indicated that PD-L1 is not only present on the surface of vesicles but also within vesicle-like structures. PD-L1-positive TEX, isolated from the supernatants of murine and human HNSCC cell lines, can impede the infiltration of CD4⁺ and CD8⁺ T cells into the tumour microenvironment, consequently expediting tumour progression (Razzo et al., 2019; Seo et al., 2018; Theodoraki et al., 2018). Moreover, to our knowledge this is the first time that the role of ADO release/produced by TEX is investigated specifically in NØ response. CD73 produces extracellular adenosine (ADO) promoting tumour growth by limiting anti-tumour T cell immunity via adenosine receptor (PIR) signalling. On the same hand, PD-L1, that acts as an immune checkpoint inhibitor for cytotoxic T lymphocytes (CTLs).

Hereby, the exchange of tumour-derived extracellular vesicles (TEX) between tumour and immune cells is crucial for cancer progression and immunomodulation. TEX have been shown to contribute to immune evasion by affecting immune functions, impairing their ability to prime effective anti-tumour responses (Rubenich et al., 2021; Whiteside, 2016). The key findings of our work demonstrate that TEX have the potential to attract NØ, interact with them, and shift the NØ phenotype from anti-tumour to a pro-tumour phenotype. Numerous studies have focused on investigating the inflammatory profile within the TME, which of particular interest is the excessive activation of NØ, whereby these cells undergo a phenotypic transformation from their canonical function to a pathogenic state (Rubenich et al., 2021). The combination of CD11b⁺/CD66⁺/CD170⁺ markers is suggested as a mean to distinguish between NØ subpopulations (Jaillon et al., 2020). The interaction involves CD73 and PD-L1, known immunosuppressive markers, influencing NØ behaviour and function. Notably, TEX induce an increase in CD170^{high}

expression and PD-L1 expression in NØ, contributing to the modulation of the immunosuppressive TME. Studies have provided evidence highlighting the significance of CD73 as a crucial regulatory molecule involved in cancer cell proliferation, migration, and invasion (Cappellari et al., 2015; Lu et al., 2022). Previous studies have examined and confirmed the concept that PD-L1 expression on NØ promotes pro-tumour characteristics (Zhang & Xu, 2017). It has been observed that PD-1 on breast cancer cells inhibits NØ cytotoxicity, whereas PD-L1^{neg} NØ possess heightened cytotoxic potential (Yajuk et al., 2021). Moreover, PD-L1^{pos} NØ have been implicated in promoting tumour growth and progression in tumours, and their presence is considered a negative prognostic factor associated with reduced patient survival (Wang et al., 2017). Moreover, NØ have been involved in modulating the TME. In the context of HNSCC, PD-L1^{pos} NØ cells have been shown to suppress T cell proliferation and activation within the inflammatory TME, consequently predicting an unfavourable prognosis. These TANs severely impair anti-tumour T cell immunity and actively contribute to tumour progression (Tang et al., 2022).

Interestingly, the PD-L1 bands detected in NØ shown in Figure 5d were with approximately 70 kDa, which is in size 20 kDa heavier than observed to date in most cell types, were PD-L1 is ranging from 45 to 55 kDa (Li et al., 2016). This specific form of PD-L1 is not well understood yet, but it is known that post-translational modifications (PTMs), such as glycosylation, phosphorylation, or ubiquitination (Ub), can increase the molecular weight of the PD-L1 protein and modulate its stability, functionality and localization (Hsu et al., 2018). There is compelling evidence suggesting that the regulation of PD-L1-mediated immunosuppression is significantly influenced by these PTMs, which directly influence PD-L1-mediated immune resistance (Hsu et al., 2018). Ubiquitination and deubiquitylation play a crucial role in the dynamics of PD-L1 protein expression, aiding tumour cells in evading immunosuppression (Hu et al., 2021; Zhou et al., 2022). Besides, a second band with 45 kDa was shown in NØ with MRS1754 in the presence of TEX, which demonstrates that blocking A_{2B}R the glycosylated canonical isoform is also present. It was reported that glycosylation of PD-L1 is important for binding to the receptor PD-1 (Shao et al., 2018).

The elevated levels of ADO in the TME are a result of increased ADO production. The deregulated ADO signalling in HNSCC creates an immunosuppressive and pro-tumour milieu (Ren et al., 2016). Conversely, the alternative pathway involves the conversion of NAD⁺ to adenosine diphosphate ribose (ADPR) facilitated by CD38. ADPR is subsequently converted to AMP by CD203a/PC-1. Both paths merge at CD73, where AMP is completely broken down into ADO (Ferretti et al., 2019). Moreover, it is imperative to acknowledge the importance of other members of ADO uptake and degradation, such as the isoenzyme adenosine deaminase (ADA) in the final amount of extracellular ADO (Gao et al., 2022). ADO, which is highly abundant in TME, exerts its immunosuppressive effects through binding to specific PIR expressed on various immune cells, including NØ. Activation of these receptors leads to the inhibition of immune cell functions, such as T cell proliferation, cytokine secretion, and cytotoxic activity (Rubenich et al., 2021). Therefore, our study aimed to understand the role of ADO signalling in NØ activation spectrum. Our data show that blocking A_{3R} led to a significant decrease in CD73 expression in the pro-tumour subpopulation and inhibited TEX modulation of PD-L1 expression. Targeting ADO signalling in immunotherapy represents a promising avenue to overcome the immunosuppressive TME and improve the effectiveness of cancer with combined treatments (Gelslechter et al., 2023).

TEX selectively modulate the cytokine profile of NØ, increasing CCL1/I-309 and Serpin E1/PAI-1 secretion. Blocking PIR reverses this effect, suggesting PIR signalling involvement. These cytokines attract immunosuppressive cells to the TME, particularly regulatory T cells (Tregs), tumour-associated macrophages (TAMs) and myeloid-derived suppressor cells (MDSCs), promoting tumour growth and immune evasion (Korbecki et al., 2020). To same extent, PAI-1 can modulate immune response by suppressing cytotoxic T cells, impairing their anti-tumour functions (Ohuchi et al., 2021). Moreover, the IHC evaluation from tumour samples corroborates with *in vitro* findings. The NØ infiltration depicts great influence in modulating lymphocyte profile. The positive correlation between NØ and Tregs both in the tumour periphery and the tumour centre clearly shows the important role of NØ in the TME immune infiltration. Indeed, a high level of NØ infiltration in solid tumours is associated with poor clinical outcomes in patients, this topic was extensively reviewed showing that not only the presence of NØ but also their specific location within the tumour is prognostically relevant (Shaul & Fridlender, 2019). Recently, it was confirmed that high intratumoral or peritumoral ratios of CD66b⁺ to CD3⁺ immune cells in liver sections from patients with hepatocellular carcinoma (HCC) are predictive of inferior overall survival (He et al., 2016). With this regard, *in vivo* experiments suggested that TANs support these processes by promoting the infiltration of macrophages (F4/80⁺) and Tregs (FoxP3⁺) within the TME (Zhou et al., 2016).

4.3 | Transition to translational research and clinical combination therapy

Immunotherapy has transformed cancer treatment tremendously. Nevertheless, it faces limitations, as only 20%–40% of patients respond, which is often due to tumour adaptability and resistance mechanisms (Ott et al., 2013; Wang et al., 2022). CD73 plays a significant role in this context, and its upregulation in the TME is linked to immunotherapy resistance (Bach et al., 2023; Thompson & Powell, 2021; Yang et al., 2021). Our data supports this observation, showing increased CD73 and PD-L1 expression in pro-tumour NØ and tumour co-culture, contributing to an immunosuppressive TME. CDK6 activation correlates with PD-L1 expression, influenced by CD73 activity. Inhibiting CD73 in pro-tumour NØ negatively affects the CD73-CyclinD-CDK4/6-PD-L1 pathway in tumour cells, suggesting a potential therapeutic strategy. The role of CDK6 in regulating PD-L1 was already

described by Zhang et al. (2018). Inhibition of CDK4/6 increases PD-L1 protein levels by interfering with Cyclin D-CDK4-mediated phosphorylation of the speckle-type POZ protein (SPOP), thereby promoting SPOP degradation. CDK4/6 activity on the other hand leads to SPOP phosphorylation, which marks PD-L1 with ubiquitin for proteasomal degradation. Interestingly, the correlation between CD73 activity and PD-L1 in tumour cells has been described as dependent of CDK6, in which extracellular ADO was found to be critical for the regulation of immune checkpoint molecules and PD-L1 levels in human macrophages, suggesting that the PTM of PD-L1 is affected by ADO. A potent selective CD73 inhibitor reversed the effects of ADO on PD-L1 (Noh et al., 2022). Our data endorse that by inhibiting CD73 with AMPCP in pro-tumour NØ, has a negative influence the CD73-Cyclin D-CDK4/6-PD-L1 pathway in tumour cells. Moreover, *in vivo* data depict the dynamic modulation of CD73/PD-L1 axis by NØ secretome. The differences between a healthy and pro-tumour response in immune cells, has a direct effect in tumour aggressiveness and immunosuppression, especially in the TME. The degradation of PD-L1 by the activation of Cyclin D-CDK4/6 signalling after inflecting NØ secretion and the reduction of CD73 expression, expresses the potential of NØ as adjuvant therapy.

Despite the similar pattern in regulating CD73-Cyclin D-CDK4/6-PD-L1 signalling in tumour cells, the modulation of the NØ pro-tumour phenotype by SCC47-derived TEX does not yield a consistent functional response in all four cell lines. Notably, SCC47 exhibited robust positive feedback when interacting with TEX primed NØ, manifesting increased migration, spreading, and reduced cell death. Conversely, SCC9 displayed a partially analogous pattern of response, while PCI52 and FaDu exhibited conflicting effects or remained unaffected. Important to point out that the *in vitro* condition is a less complex environment and the interaction with NØ varies between the non-modulated (+NØ) and TEX-modulated NØ (+TEX). The co-incubation culture provides information about the response to the stimuli, and, in this experimental design, we focused our evaluation in comparing the tumour response to healthy non-stimulated NØ and pro-tumour TEX-induced NØ. With this regard, TEX exhibit cell line-specific effects on NØ, highlighting the unique responsiveness of each cell line to external stimuli. This variability emphasizes the need for personalized therapeutic approaches in cancer treatment. To that extent, the very heterogeneity that facilitates TEX utility also presents a challenge in the development of drug delivery systems reliant on exosomes (Chen et al., 2022). Furthermore, this variability may elucidate why conventional treatments involving immune cell modulation or exosome-targeted therapies exhibit efficacy in a limited subset of patients, emphasizing the necessity for personalized therapeutic approaches. With this regard, further studies need to be conducted in order to understand the full impact of the target mechanism associated with NØ polarization.

Targeted therapies involving CD39 or CD73 alongside anti-PD-1 or anti-PD-L1 show promise in pre-clinical and clinical studies (Laubach et al., 2023). A recent report on a phase I clinical trial involving anti-CD73 and anti-PD-L1 revealed tolerable safety profiles and moderate efficacy (Bendell et al., 2023). Phase II trials targeting CD73, especially in combination with anti-PD-L1, demonstrate enhanced response rates (Chang & Hao, 2022; Herbst et al., 2022). In our study, we propose the use of NØ as therapeutic target, with special regard to A3R as a key player in the activation spectrum. NØ have been proposed as cancer targets due to the easiness in infiltrating TME and cell communication (Granot, 2019; Linde et al., 2023; Raskov et al., 2022). Amidst ongoing investigations into combinations of diverse treatments and additional checkpoint targets, a profound understanding of the TME remains imperative for the advancement of novel therapeutic strategies.

5 | CONCLUSION

Our study reveals significant insights into the crosstalk between HNSCC-derived extracellular vesicles (TEX) and neutrophils (NØ) within the tumour microenvironment (TME), which is summarized in Figure 8. In conclusion, the comprehensive analysis of NLR and PD-L1 dynamics in tumorigenesis has provided valuable insights into the intricate interplay between immune markers and TME. Elevated NLR, indicative of systemic inflammation, has been consistently linked to poor prognosis in various cancers, emphasizing its potential as a diagnostic and predictive tool. The investigation into PD-L1 expression, particularly its subcellular localization, has revealed a nuanced relationship with tumour aggressiveness, with variations in membrane and cytoplasmic localization linked to differing NLR values.

The study delves into the role of TEX in orchestrating immunosuppression within the TME, highlighting their ability to induce a pro-tumour NØ phenotype. The presence of immunosuppressive factors, including CD73 and PD-L1, in TEX underscores their role in shaping the immune landscape. Moreover, the study elucidates the potential of TEX to modulate cytokine profiles and influence the behaviour of immune cells, particularly NØ. We demonstrated that TEX promote NØ chemotaxis and attachment, leading to a shift in NØ phenotype characterized by increased CD170^{high}, CD73^{pos}, and cPD-L1 expressions, indicative of a pro-tumour transformation. This TEX-induced phenotype modulates the NØ cytokine release profile, enhancing the secretion of immunosuppressive factors like CCL1/I-309 and Serpin E1/PAI-1. Our data underscore the pivotal role of adenosine (ADO) signalling in these processes, suggesting that targeting ADO signalling, especially A3R, could be a promising approach to counteract the immunosuppressive TANs and boost the effectiveness of cancer treatments.

The transition to translational research and clinical combination therapy was discussed, emphasizing the significance of targeting CD73 and PD-L1 concurrently, especially in the context of immunotherapy resistance. The findings support the notion that understanding the dynamic modulation of CD73/PD-L1 axis by NØ could serve as a potential adjuvant therapy, offering

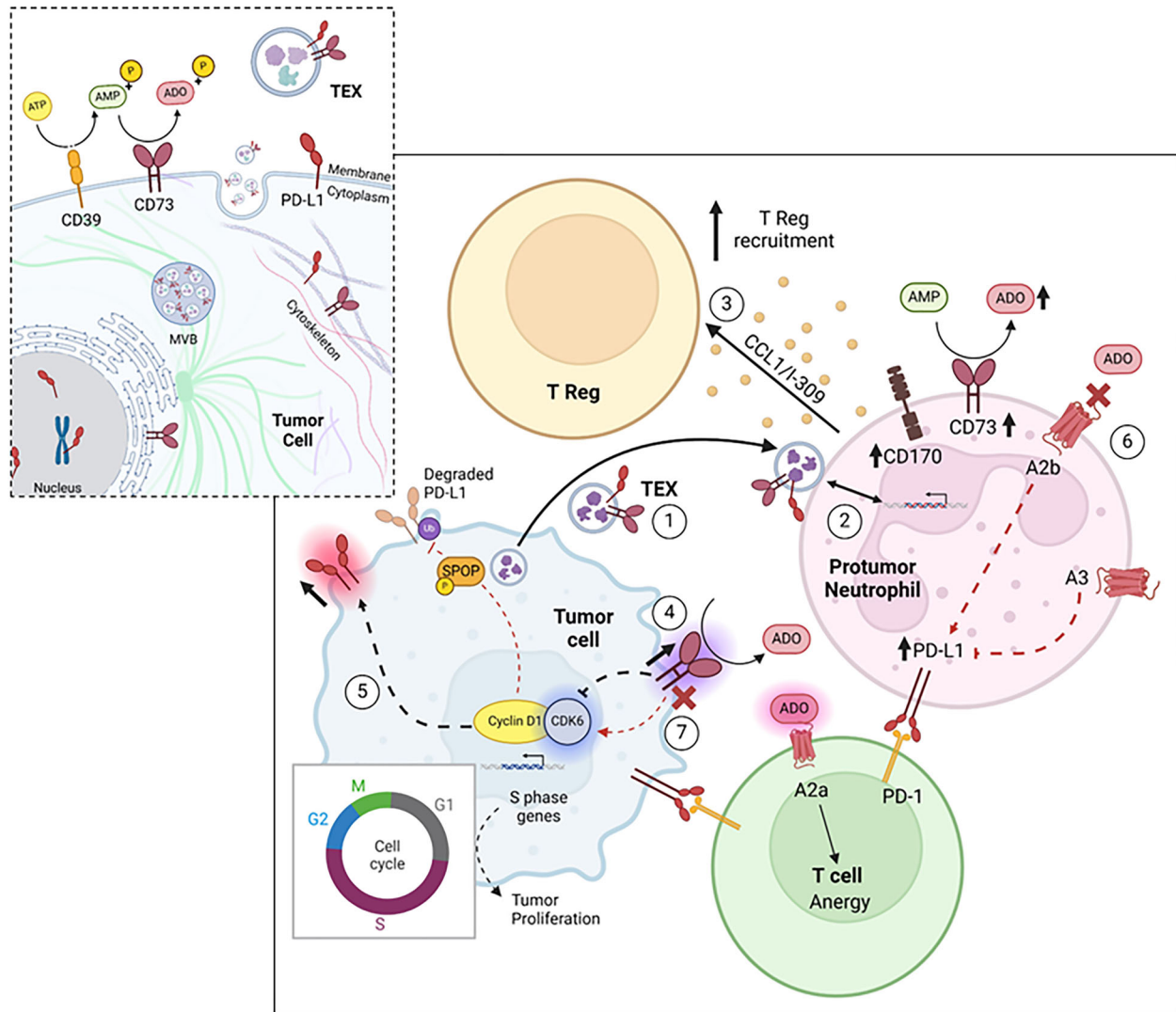


FIGURE 8 The role of tumour-derived extracellular vesicles and neutrophils in orchestrating the dynamic CD73/PD-L1 axis in HNC. (1) Tumour cells secrete TEX carrying immunosuppressive factors, such as PD-L1 and active ADO producing enzyme, CD73. (2) TEX interact with NØ inducing a pro-tumour phenotype by increasing expression of CD170, CD73 and PD-L1. (3) Pro-tumour NØ secrete immunosuppressive cytokines, recruiting Tregs. (4) Extracellular ADO is increased and upregulates CD73 activity on tumour cells. (5) CD73 expression inhibits Cyclin D1-CDK4/6, and therefore, increases PD-L1 expression in tumour cells. (6) By blocking PIR on NØ, the phenotype is modulated: A2_BR acts synergistic to exosome influence and potentiates the pro-tumour phenotype. A3R inhibits the pro-tumour phenotype by reducing CD73 and PD-L1 expression. (7) The reduced ADO and immunosuppressive TME downregulate CD73, which activates Cyclin D1-CDK4/6 signalling, phosphorylating SPOP, resulting in the degradation of PD-L1. SPOP, speckle-type POZ protein; TME, tumour microenvironment.

insights into the complex regulatory mechanisms underlying immunosuppression. However, the variability in responses to TEX among different cell lines underscores the challenges in developing universally effective therapeutic approaches.

This study contributes significantly to our understanding of the complex interactions within the TME, featuring the potential therapeutic avenues for cancer treatment. The emphasis on personalized approaches and the exploration of novel targets underscores the importance of continued research in unravelling the intricacies of tumour-immune cross-modulation for the development of more effective and tailored cancer therapies.

AUTHOR CONTRIBUTIONS

Dominique S. Rubenich: Conceptualization; data curation; formal analysis; investigation; methodology; project administration; supervision; visualization; writing—original draft; writing—review and editing. **Jordana L. Domagalski:** Formal analysis; writing—review and editing. **Gabriela F. S. Gentil:** Formal analysis; writing—review and editing. **Jonas Eichberger:** Data curation; writing—review and editing. **Mathias Fiedler:** Data curation; writing—review and editing. **Florian Weber:** Data curation; formal analysis. **Marianne Federlin:** Data curation; resources. **Hendrik Poeck:** Data curation; resources. **Torsten E. Reichert:** Funding acquisition; resources. **Tobias Ettl:** Data curation; funding acquisition; resources. **Richard J. Bauer:** Funding acquisition;

resources; supervision; writing—review and editing. **Elizandra Braganhol**: Conceptualization; supervision; writing—review and editing. **Daniela Schulz**: Data curation; formal analysis; investigation; methodology; project administration; supervision; validation; visualization; writing—review and editing.

ACKNOWLEDGEMENTS

This work was supported by Deutsche Forschungsgemeinschaft (DFG, GZ: 3696/7-1), Conselho Nacional de Desenvolvimento Científico e Tecnológico (CNPq – 142520/2020-9), CAPES & Deutscher Akademischer Austauschdienst (CAPES: 88881.895087/2023-01, DAAD: 57705675) and University Hospital Regensburg (UKR). We thank Maxi Bleicher, Gabriele Schöhammer, Gerlinde Ferstl, Niklas Wenzl and Rudolf Jung for their excellent technical assistance as well as Sophia Rohrmüller, Dr. Nicole Schäfer and Dr. Petra Hoffmann for their valuable support.

CONSENT FOR PUBLICATION

All authors agreement with the content of the manuscript and with the submission.

CONFLICT OF INTEREST STATEMENT

The authors declare no conflicts of interest.

ORCID

Dominique S. Rubenich  <https://orcid.org/0000-0002-5108-4350>

Jordana L. Domagalski  <https://orcid.org/0000-0001-8804-9826>

Gabriela F. S. Gentil  <https://orcid.org/0000-0003-3611-6622>

Elizandra Braganhol  <https://orcid.org/0000-0002-9105-3858>

Daniela Schulz  <https://orcid.org/0009-0007-6584-1715>

REFERENCES

- Allard, B., Longhi, M. S., Robson, S. C., & Stagg, J. (2017). The ectonucleotidases CD39 and CD73: Novel checkpoint inhibitor targets. *Immunological Reviews*, 276(1), 121–144. <https://doi.org/10.1111/imr.12528>
- Allard, D., Chrobak, P., Allard, B., Messaoudi, N., & Stagg, J. (2019). Targeting the CD73-adenosine axis in immuno-oncology. *Immunology Letters*, 205, 31–39. <https://doi.org/10.1016/j.imlet.2018.05.001>
- Bach, N., Winzer, R., Tolosa, E., Fiedler, W., & Brauneck, F. (2023). The clinical significance of CD73 in cancer. *International Journal of Molecular Sciences*, 24(14), 11759. <https://doi.org/10.3390/ijms241411759>
- Bendell, J., LoRusso, P., Overman, M., Noonan, A. M., Kim, D. W., Strickler, J. H., Kim, S. W., Clarke, S., George, T. J., Grimison, P. S., Barve, M., Amin, M., Desai, J., Wise-Draper, T., Eck, S., Jiang, Y., Khan, A. A., Wu, Y., Martin, P., ... Patel, S. P. (2023). First-in-human study of oleclumab, a potent, selective anti-CD73 monoclonal antibody, alone or in combination with durvalumab in patients with advanced solid tumors. *Cancer Immunology, Immunotherapy: CII*, 72(7), 2443–2458. <https://doi.org/10.1007/s00262-023-03430-6>
- Boussiotis, V. A. (2016). Molecular and biochemical aspects of the PD-1 checkpoint pathway. *The New England Journal of Medicine*, 375(18), 1767–1778. <https://doi.org/10.1056/NEJMra1514296>
- Cappellari, A. R., Pillat, M. M., Souza, H. D., Dietrich, F., Oliveira, F. H., Figueiró, F., Abujamra, A. L., Roesler, R., Lecka, J., Sévigny, J., Battastini, A. M., & Ulrich, H. (2015). Ecto-5'-nucleotidase overexpression reduces tumor growth in a xenograph medulloblastoma model. *PLoS ONE*, 10(10), e0140996. <https://doi.org/10.1371/journal.pone.0140996>
- Carus, A., Ladekarl, M., Hager, H., Pilegaard, H., Nielsen, P. S., & Donskov, F. (2013). Tumor-associated neutrophils and macrophages in non-small cell lung cancer: No immediate impact on patient outcome. *Lung Cancer*, 81(1), 130–137. <https://doi.org/10.1016/j.lungcan.2013.03.003>
- Chang, A., & Hao, J. (2022). A tumor intrinsic role of CD73 in pancreatic adenocarcinoma. *Annals of Pancreatic Cancer*, 5, 9. <https://doi.org/10.21037/APC-2022-2>
- Chen, L., Wang, L., Zhu, L., Xu, Z., Liu, Y., Li, Z., Zhou, J., & Luo, F. (2022). Exosomes as drug carriers in anti-cancer therapy. *Frontiers in Cell and Developmental Biology*, 10, 728616. <https://doi.org/10.3389/fcell.2022.728616>
- Chen, L., Xiong, Y., Li, J., Zheng, X., Zhou, Q., Turner, A., Wu, C., Lu, B., & Jiang, J. (2017). PD-L1 expression promotes epithelial to mesenchymal transition in human esophageal cancer. *Cellular Physiology and Biochemistry*, 42(6), 2267–2280. <https://doi.org/10.1159/000480000>
- Chen, Y., Corriden, R., Inoue, Y., Yip, L., Hashiguchi, N., Zinkernagel, A., Nizet, V., Insel, P. A., & Junger, W. G. (2006). ATP release guides neutrophil chemotaxis via P2Y2 and A3 receptors. *Science*, 314(5806), 1792–1795. <https://doi.org/10.1126/science.1132559>
- Clayton, A., Al-Taei, S., Webber, J., Mason, M. D., & Tabi, Z. (2011). Cancer exosomes express CD39 and CD73, which suppress T cells through adenosine production. *Journal of Immunology*, 187(2), 676–683. <https://doi.org/10.4049/jimmunol.1003884>
- Daassi, D., Mahoney, K. M., & Freeman, G. J. (2020). The importance of exosomal PDL1 in tumour immune evasion. *Nature Reviews Immunology*, 20(4), 209–215. <https://doi.org/10.1038/s41577-019-0264-y>
- Demeules, M., Scarpitta, A., Harget, R., Gondé, H., Abad, C., Blandin, M., Menzel, S., Duan, Y., Rissiek, B., Magnus, T., Mann, A. M., Koch-Nolte, F., & Adriouch, S. (2022). Evaluation of nanobody-based biologics targeting purinergic checkpoints in tumor models *in vivo*. *Frontiers in Immunology*, 13, 1012534. <https://doi.org/10.3389/fimmu.2022.1012534>
- Deng, W. W., Li, Y. C., Ma, S. R., Mao, L., Yu, G. T., Bu, L. L., Kulkarni, A. B., Zhang, W. F., & Sun, Z. J. (2018). Specific blockade CD73 alters the “exhausted” phenotype of T cells in head and neck squamous cell carcinoma. *International Journal of Cancer*, 143(6), 1494–1504. <https://doi.org/10.1002/ijc.31534>
- Eichberger, J., Schulz, D., Pscheidl, K., Fiedler, M., Reichert, T. E., Bauer, R. J., & Ettl, T. (2020). PD-L1 influences cell spreading, migration and invasion in head and neck cancer cells. *International Journal of Molecular Sciences*, 21(21), 8089. <https://doi.org/10.3390/ijms21218089>
- Elmusrati, A., Wang, J., & Wang, C. Y. (2021). Tumor microenvironment and immune evasion in head and neck squamous cell carcinoma. *International Journal of Oral Science*, 13(1), 24. <https://doi.org/10.1038/s41368-021-00131-7>

- Ettl, T., Grube, M., Schulz, D., & Bauer, R. J. (2022). Checkpoint inhibitors in cancer therapy: clinical benefits for head and neck cancers. *Cancers*, *14*(20), 4985. <https://doi.org/10.3390/cancers14204985>
- Ferretti, E., Horenstein, A. L., Canzonetta, C., Costa, F., & Morandi, F. (2019). Canonical and non-canonical adenosine pathways. *Immunology Letters*, *205*, 25–30. <https://doi.org/10.1016/j.imlet.2018.03.007>
- Gao, Z. W., Yang, L., Liu, C., Wang, X., Guo, W. T., Zhang, H. Z., & Dong, K. (2022). Distinct roles of adenosine deaminase isoenzymes ADA1 and ADA2: A pan-cancer analysis. *Frontiers in Immunology*, *13*, 903461. <https://doi.org/10.3389/fimmu.2022.903461>
- Gato-Cañas, M., Zuazo, M., Arasanz, H., Ibañez-Vea, M., Lorenzo, L., Fernandez-Hinojal, G., Vera, R., Smerdou, C., Martisova, E., Arozarena, I., Wellbrock, C., Llopiz, D., Ruiz, M., Sarobe, P., Breckpot, K., Kochan, G., & Escors, D. (2017). PDL1 signals through conserved sequence motifs to overcome interferon-mediated cytotoxicity. *Cell Reports*, *20*(8), 1818–1829. <https://doi.org/10.1016/j.celrep.2017.07.075>
- Gelsleichter, N. E., Azambuja, J. H., Rubenich, D. S., & Braganhol, E. (2023). CD73 in glioblastoma: Where are we now and what are the future directions? *Immunology Letters*, *256–257*, 20–27. <https://doi.org/10.1016/j.imlet.2023.03.005>
- Giuliani, A. L., Sarti, A. C., & Di Virgilio, F. (2021). Ectonucleotidases in acute and chronic inflammation. *Frontiers in Pharmacology*, *11*, 619458. <https://doi.org/10.3389/fphar.2020.619458>
- Granot, Z. (2019). Neutrophils as a therapeutic target in cancer. *Frontiers in Immunology*, *10*, 1710. <https://doi.org/10.3389/fimmu.2019.01710>
- Gurunathan, S., Kang, M. H., Jeyaraj, M., Qasim, M., & Kim, J. H. (2019). Review of the isolation, characterization, biological function, and multifarious therapeutic approaches of exosomes. *Cells*, *8*(4), 307. <https://doi.org/10.3390/cells8040307>
- Haas, L., & Obenauf, A. C. (2019). Allies or enemies—the multifaceted role of myeloid cells in the tumor microenvironment. *Frontiers in Immunology*, *10*, 2746. <https://doi.org/10.3389/fimmu.2019.02746>
- He, M., Peng, A., Huang, X. Z., Shi, D. C., Wang, J. C., Zhao, Q., Lin, H., Kuang, D. M., Ke, P. F., & Lao, X. M. (2016). Peritumoral stromal neutrophils are essential for c-Met-elicited metastasis in human hepatocellular carcinoma. *Oncoimmunology*, *5*(10), e1219828. <https://doi.org/10.1080/2162402X.2016.1219828>
- Herbst, R. S., Majem, M., Barlesi, F., Carcereny, E., Chu, Q., Monnet, I., Sanchez-Hernandez, A., Dakhil, S., Camidge, D. R., Winzer, L., Soo-Hoo, Y., Cooper, Z. A., Kumar, R., Bothos, J., Aggarwal, C., & Martinez-Marti, A. (2022). COAST: An open-label, phase ii, multidrug platform study of durvalumab alone or in combination with oleclumab or monalizumab in patients with unresectable, stage III non-small-cell lung cancer. *Journal of Clinical Oncology*, *40*(29), 3383–3393. <https://doi.org/10.1200/JCO.22.00227>
- Hsu, C. C., Chou, W. C., Hung, Y. S., Lin, S. Y., Hung, C. Y., Yeh, K. Y., Wang, H. M., & Lu, C. H. (2022). Predictive value of albumin and neutrophil-to-lymphocyte ratio score for treatment completeness and safety profiles in patients with head and neck cancer receiving definitive concurrent chemoradiotherapy. *In vivo*, *36*(6), 2875–2883. <https://doi.org/10.21873/invivo.13028>
- Hsu, J. M., Li, C. W., Lai, Y. J., & Hung, M. C. (2018). Posttranslational modifications of PD-L1 and their applications in cancer therapy. *Cancer Research*, *78*(22), 6349–6353. <https://doi.org/10.1158/0008-5472.CAN-18-1892>
- Hu, X., Wang, J., Chu, M., Liu, Y., Wang, Z. W., & Zhu, X. (2021). Emerging role of ubiquitination in the regulation of PD-1/PD-L1 in cancer immunotherapy. *Molecular Therapy: The Journal of the American Society of Gene Therapy*, *29*(3), 908–919. <https://doi.org/10.1016/j.ymthe.2020.12.032>
- Jaillon, S., Ponzetta, A., Di Mitri, D., Santoni, A., Bonecchi, R., & Mantovani, A. (2020). Neutrophil diversity and plasticity in tumour progression and therapy. *Nature Reviews Cancer*, *20*(9), 485–503. <https://doi.org/10.1038/s41568-020-0281-y>
- Korbecki, J., Grochans, S., Gutowska, I., Barczak, K., & Baranowska-Bosiacka, I. (2020). CC chemokines in a tumor: a review of pro-cancer and anti-cancer properties of receptors CCR5, CCR6, CCR7, CCR8, CCR9, and CCR10 ligands. *International Journal of Molecular Sciences*, *21*(20), 7619. <https://doi.org/10.3390/ijms21207619>
- Laubach, K., Turan, T., Mathew, R., Wilsbacher, J., Engelhardt, J., & Samayoa, J. (2023). Tumor-intrinsic metabolic reprogramming and how it drives resistance to anti-PD-1/PD-L1 treatment. *Cancer Drug Resistance*, *6*(3), 611–641. <https://doi.org/10.20517/cdr.2023.60>
- Leemans, C. R., Snijders, P. J. F., & Brakenhoff, R. H. (2018). The molecular landscape of head and neck cancer. *Nature Reviews Cancer*, *18*(5), 269–282. <https://doi.org/10.1038/nrc.2018.11>
- Li, C. W., Lim, S. O., Xia, W., Lee, H. H., Chan, L. C., Kuo, C. W., Khoo, K. H., Chang, S. S., Cha, J. H., Kim, T., Hsu, J. L., Wu, Y., Hsu, J. M., Yamaguchi, H., Ding, Q., Wang, Y., Yao, J., Lee, C. C., Wu, H. J., ... Hung, M. C. (2016). Glycosylation and stabilization of programmed death ligand-1 suppresses T-cell activity. *Nature Communications*, *7*, 12632. <https://doi.org/10.1038/ncomms12632>
- Lin, C. J., Grandis, J. R., Carey, T. E., Gollin, S. M., Whiteside, T. L., Koch, W. M., Ferris, R. L., & Lai, S. Y. (2007). Head and neck squamous cell carcinoma cell lines: Established models and rationale for selection. *Head & Neck*, *29*(2), 163–188. <https://doi.org/10.1002/hed.20478>
- Linde, I. L., Prestwood, T. R., Qiu, J., Pilarowski, G., Linde, M. H., Zhang, X., Shen, L., Reticker-Flynn, N. E., Chiu, D. K., Sheu, L. Y., Van Deursen, S., Tolentino, L. L., Song, W. C., & Engleman, E. G. (2023). Neutrophil-activating therapy for the treatment of cancer. *Cancer Cell*, *41*(2), 356–372. e10. <https://doi.org/10.1016/j.ccell.2023.01.002>
- Lu, T., Zhang, Z., Zhang, J., Pan, X., Zhu, X., Wang, X., Li, Z., Ruan, M., Li, H., Chen, W., & Yan, M. (2022). CD73 in small extracellular vesicles derived from HNSCC defines tumour-associated immunosuppression mediated by macrophages in the microenvironment. *Journal of Extracellular Vesicles*, *11*(5), e12218. <https://doi.org/10.1002/jev2.12218>
- Ludwig, N., Razzo, B. M., Yerneni, S. S., & Whiteside, T. L. (2019). Optimization of cell culture conditions for exosome isolation using mini-size exclusion chromatography (mini-SEC). *Experimental Cell Research*, *378*(2), 149–157. <https://doi.org/10.1016/j.yexcr.2019.03.014>
- Ludwig, N., Rubenich, D. S., Zaręba, Ł., Siewiera, J., Pieper, J., Braganhol, E., Reichert, T. E., & Szczepański, M. J. (2020). Potential roles of tumor cell- and stroma cell-derived small extracellular vesicles in promoting a pro-angiogenic tumor microenvironment. *Cancers*, *12*(12), 3599. <https://doi.org/10.3390/cancers12123599>
- Ludwig, N., Yerneni, S. S., Azambuja, J. H., Gillespie, D. G., Menshikova, E. V., Jackson, E. K., & Whiteside, T. L. (2020). Tumor-derived exosomes promote angiogenesis via adenosine A_{2B} receptor signaling. *Angiogenesis*, *23*(4), 599–610. <https://doi.org/10.1007/s10456-020-09728-8>
- Mascarella, M. A., Mannard, E., Silva, S. D., & Zeitouni, A. (2018). Neutrophil-to-lymphocyte ratio in head and neck cancer prognosis: A systematic review and meta-analysis. *Head & Neck*, *40*(5), 1091–1100. <https://doi.org/10.1002/hed.25075>
- Masucci, M. T., Minopoli, M., & Carriero, M. V. (2019). Tumor associated neutrophils. Their role in tumorigenesis, metastasis, prognosis and therapy. *Frontiers in Oncology*, *9*, 1146. <https://doi.org/10.3389/fonc.2019.01146>
- Minciacchi, V. R., Freeman, M. R., & Di Vizio, D. (2015). Extracellular vesicles in cancer: Exosomes, microvesicles and the emerging role of large oncosomes. *Seminars in Cell & Developmental Biology*, *40*, 41–51. <https://doi.org/10.1016/j.semcdb.2015.02.010>
- Mortezaei, K. (2020). Immune escape: A critical hallmark in solid tumors. *Life Sciences*, *258*, 118110. <https://doi.org/10.1016/j.lfs.2020.118110>
- Niu, M., Liu, Y., Yi, M., Jiao, D., & Wu, K. (2022). Biological characteristics and clinical significance of soluble PD-1/PD-L1 and exosomal PD-L1 in cancer. *Frontiers in Immunology*, *13*, 827921. <https://doi.org/10.3389/fimmu.2022.827921>

- Noh, J. Y., Lee, I. P., Han, N. R., Kim, M., Min, Y. K., Lee, S. Y., Yun, S. H., Kim, S. I., Park, T., Chung, H., Park, D., & Lee, C. H. (2022). Additive effect of CD73 inhibitor in colorectal cancer treatment with CDK4/6 inhibitor through regulation of PD-L1. *Cellular and Molecular Gastroenterology and Hepatology*, 14(4), 769–788. <https://doi.org/10.1016/j.jcmgh.2022.07.005>
- Oh, H., Siano, B., & Diamond, S. (2008). Neutrophil isolation protocol. *Journal of Visualized Experiments: JoVE*, 17, 745. <https://doi.org/10.3791/745>
- Ohuchi, K., Kambayashi, Y., Hidaka, T., & Fujimura, T. (2021). Plasminogen activating inhibitor-1 might predict the efficacy of anti-PD1 antibody in advanced melanoma patients. *Frontiers in Oncology*, 11, 798385. <https://doi.org/10.3389/fonc.2021.798385>
- Ott, P. A., Hodi, F. S., & Robert, C. (2013). CTLA-4 and PD-1/PD-L1 blockade: New immunotherapeutic modalities with durable clinical benefit in melanoma patients. *Clinical Cancer Research: An Official Journal of the American Association for Cancer Research*, 19(19), 5300–5309. <https://doi.org/10.1158/1078-0432.CCR-13-0143>
- Raskov, H., Orhan, A., Gaggari, S., & Gögenur, I. (2022). Neutrophils and polymorphonuclear myeloid-derived suppressor cells: An emerging battleground in cancer therapy. *Oncogenesis*, 11(1), 22. <https://doi.org/10.1038/s41389-022-00398-3>
- Razzo, B. M., Ludwig, N., Hong, C. S., Sharma, P., Fabian, K. P., Fecek, R. J., Storkus, W. J., & Whiteside, T. L. (2019). Tumor-derived exosomes promote carcinogenesis of murine oral squamous cell carcinoma. *Carcinogenesis*, 41(5), 625–633. <https://doi.org/10.1093/carcin/bgz124>
- Ren, Z. H., Lin, C. Z., Cao, W., Yang, R., Lu, W., Liu, Z. Q., Chen, Y. M., Yang, X., Tian, Z., Wang, L. Z., Li, J., Wang, X., Chen, W. T., Ji, T., & Zhang, C. P. (2016). CD73 is associated with poor prognosis in HNSCC. *Oncotarget*, 7(38), 61690–61702. <https://doi.org/10.18632/oncotarget.11435>
- Rubenich, D. S., de Souza, P. O., Omizzollo, N., Aubin, M. R., Basso, P. J., Silva, L. M., da Silva, E. M., Teixeira, F. C., Gentil, G. F. S., Domagalski, J. L., Cunha, M. T., Gadelha, K. A., Diel, L. F., Gelsleichter, N. E., Rubenich, A. S., Lenz, G. S., de Abreu, A. M., Kroeff, G. M., Paz, A. H., ... Braganhol, E. (2023). Tumor-neutrophil crosstalk promotes *in vitro* and *in vivo* glioblastoma progression. *Frontiers in Immunology*, 14, 1183465. <https://doi.org/10.3389/fimmu.2023.1183465>
- Rubenich, D. S., de Souza, P. O., Omizzollo, N., Lenz, G. S., Sevigny, J., & Braganhol, E. (2021). Neutrophils: Fast and furious—the nucleotide pathway. *Purinergic Signalling*, 17(3), 371–383. <https://doi.org/10.1007/s11302-021-09786-7>
- Rubenich, D. S., Omizzollo, N., Szczepański, M. J., Reichert, T. E., Whiteside, T. L., Ludwig, N., & Braganhol, E. (2021). Small extracellular vesicle-mediated bidirectional crosstalk between neutrophils and tumor cells. *Cytokine & Growth Factor Reviews*, 61, 16–26. <https://doi.org/10.1016/j.cytogfr.2021.08.002>
- Schulz, D., Feulner, L., Santos Rubenich, D., Heimer, S., Rohrmüller, S., Reinders, Y., Falchetti, M., Wetzel, M., Braganhol, E., Lummertz da Rocha, E., Schäfer, N., Stöckl, S., Brockhoff, G., Wege, A. K., Fritsch, J., Pohl, F., Reichert, T. E., Ettl, T., & Bauer, R. J. (2024). Subcellular localization of PD-L1 and cell-cycle-dependent expression of nuclear PD-L1 variants: Implications for head and neck cancer cell functions and therapeutic efficacy. *Molecular Oncology*, 18(2), 431–452. <https://doi.org/10.1002/1878-0261.13567>
- Schulz, D., Stancev, I., Sorrentino, A., Meneve, A. N., Beckhove, P., Brockhoff, G., Hautmann, M. G., Reichert, T. E., Bauer, R. J., & Ettl, T. (2019). Increased PD-L1 expression in radioresistant HNSCC cell lines after irradiation affects cell proliferation due to inactivation of GSK-3beta. *Oncotarget*, 10(5), 573–583. <https://doi.org/10.18632/oncotarget.26542>
- Schulz, D., Wetzel, M., Eichberger, J., Piendl, G., Brockhoff, G., Wege, A. K., Reichert, T. E., Ettl, T., & Bauer, R. J. (2021). Differential expression of PD-L1 during cell cycle progression of head and neck squamous cell carcinoma. *International Journal of Molecular Sciences*, 22(23), 13087. <https://doi.org/10.3390/ijms222313087>
- Seo, N., Akiyoshi, K., & Shiku, H. (2018). Exosome-mediated regulation of tumor immunology. *Cancer Science*, 109(10), 2998–3004. <https://doi.org/10.1111/cas.13735>
- Shao, B., Li, C. W., Lim, S. O., Sun, L., Lai, Y. J., Hou, J., Liu, C., Chang, C. W., Qiu, Y., Hsu, J. M., Chan, L. C., Zha, Z., Li, H., & Hung, M. C. (2018). Deglycosylation of PD-L1 by 2-deoxyglucose reverses PARP inhibitor-induced immunosuppression in triple-negative breast cancer. *American Journal of Cancer Research*, 8(9), 1837–1846.
- Shaul, M. E., & Fridlender, Z. G. (2019). Tumour-associated neutrophils in patients with cancer. *Nature Reviews Clinical Oncology*, 16(10), 601–620. <https://doi.org/10.1038/s41571-019-0222-4>
- Sung, H., Ferlay, J., Siegel, R. L., Laversanne, M., Soerjomataram, I., Jemal, A., & Bray, F. (2021). Global cancer statistics 2020: GLOBOCAN estimates of incidence and mortality worldwide for 36 cancers in 185 countries. *CA: A Cancer Journal for Clinicians*, 71(3), 209–249. <https://doi.org/10.3322/caac.21660>
- Takenaka, Y., Oya, R., Takemoto, N., & Inohara, H. (2022). Neutrophil-to-lymphocyte ratio as a prognostic marker for head and neck squamous cell carcinoma treated with immune checkpoint inhibitors: Meta-analysis. *Head & Neck*, 44(5), 1237–1245. <https://doi.org/10.1002/hed.26997>
- Tang, D., Zhang, D., Heng, Y., Zhu, X. K., Lin, H. Q., Zhou, J., Tao, L., & Lu, L. M. (2022). Tumor-infiltrating PD-L1+ neutrophils induced by GM-CSF suppress T cell function in laryngeal squamous cell carcinoma and predict unfavorable prognosis. *Journal of Inflammation Research*, 15, 1079–1097. <https://doi.org/10.2147/JIR.S347777>
- Tang, Y., Zhang, P., Wang, Y., Wang, J., Su, M., Wang, Y., Zhou, L., Zhou, J., Xiong, W., Zeng, Z., Zhou, Y., Nie, S., & Liao, Q. (2020). The biogenesis, biology, and clinical significance of exosomal PD-L1 in cancer. *Frontiers in Immunology*, 11, 604. <https://doi.org/10.3389/fimmu.2020.00604>
- Theodoraki, M. N., Yerneni, S. S., Hoffmann, T. K., Gooding, W. E., & Whiteside, T. L. (2018). Clinical significance of PD-L1+ exosomes in plasma of head and neck cancer patients. *Clinical Cancer Research: An Official Journal of the American Association for Cancer Research*, 24(4), 896–905. <https://doi.org/10.1158/1078-0432.CCR-17-2664>
- Théry, C., Witwer, K. W., Aikawa, E., Alcaraz, M. J., Anderson, J. D., Andriantsitohaina, R., Antoniou, A., Arab, T., Archer, F., Atkin-Smith, G. K., Ayre, D. C., Bach, J. M., Bachurski, D., Baharvand, H., Balaj, L., Baldacchino, S., Bauer, N. N., Baxter, A. A., Bebawy, M., ... Zuba-Surma, E. K. (2018). Minimal information for studies of extracellular vesicles 2018 (MISEV2018): A position statement of the International Society for Extracellular Vesicles and update of the MISEV2014 guidelines. *Journal of Extracellular Vesicles*, 7(1), 1535750. <https://doi.org/10.1080/20013078.2018.1535750>
- Thompson, E. A., & Powell, J. D. (2021). Inhibition of the adenosine pathway to potentiate cancer immunotherapy: Potential for combinatorial approaches. *Annual Review of Medicine*, 72, 331–348. <https://doi.org/10.1146/annurev-med-060619-023155>
- Wang, T. T., Zhao, Y. L., Peng, L. S., Chen, N., Chen, W., Lv, Y. P., Mao, F. Y., Zhang, J. Y., Cheng, P., Teng, Y. S., Fu, X. L., Yu, P. W., Guo, G., Luo, P., Zhuang, Y., & Zou, Q. M. (2017). Tumour-activated neutrophils in gastric cancer foster immune suppression and disease progression through GM-CSF-PD-L1 pathway. *Gut*, 66(11), 1900–1911. <https://doi.org/10.1136/gutjnl-2016-313075>
- Wang, Y., Zhang, H., Liu, C., Wang, Z., Wu, W., Zhang, N., Zhang, L., Hu, J., Luo, P., Zhang, J., Liu, Z., Peng, Y., Liu, Z., Tang, L., & Cheng, Q. (2022). Immune checkpoint modulators in cancer immunotherapy: Recent advances and emerging concepts. *Journal of Hematology & Oncology*, 15(1), 111. <https://doi.org/10.1186/s13045-022-01325-0>
- Whiteside, T. L. (2016). Tumor-Derived exosomes and their role in cancer progression. *Advances in Clinical Chemistry*, 74, 103–141. <https://doi.org/10.1016/bs.acc.2015.12.005>
- Yajuk, O., Baron, M., Tokar, S., Zelter, T., Fainsod-Levi, T., & Granot, Z. (2021). The PD-L1/PD-1 axis blocks neutrophil cytotoxicity in cancer. *Cells*, 10(6), 1510. <https://doi.org/10.3390/cells10061510>
- Yang, H., Yao, F., Davis, P. F., Tan, S. T., & Hall, S. R. R. (2021). CD73, tumor plasticity and immune evasion in solid cancers. *Cancers*, 13(2), 177. <https://doi.org/10.3390/cancers13020177>

- Ye, J., Gavras, N. W., Keeley, D. C., Hughson, A. L., Hannon, G., Vrooman, T. G., Lesch, M. L., Johnston, C. J., Lord, E. M., Belt, B. A., Linehan, D. C., Eyles, J., & Gerber, S. A. (2023). CD73 and PD-L1 dual blockade amplifies antitumor efficacy of SBRT in murine PDAC models. *Journal for Immunotherapy of Cancer*, *11*(5), e006842. <https://doi.org/10.1136/jitc-2023-006842>
- Zhang, J., Bu, X., Wang, H., Zhu, Y., Geng, Y., Nihira, N. T., Tan, Y., Ci, Y., Wu, F., Dai, X., Guo, J., Huang, Y. H., Fan, C., Ren, S., Sun, Y., Freeman, G. J., Sicinski, P., & Wei, W. (2018). Cyclin D-CDK4 kinase destabilizes PD-L1 via cullin 3-SPOP to control cancer immune surveillance. *Nature*, *553*(7686), 91–95. <https://doi.org/10.1038/nature25015>
- Zhang, S., Yang, X., Wang, L., & Zhang, C. (2018). Interplay between inflammatory tumor microenvironment and cancer stem cells. *Oncology Letters*, *16*(1), 679–686. <https://doi.org/10.3892/ol.2018.8716>
- Zhang, X., & Xu, W. (2017). Neutrophils diminish T-cell immunity to foster gastric cancer progression: The role of GM-CSF/PD-L1/PD-1 signalling pathway. *Gut*, *66*(11), 1878–1880. <https://doi.org/10.1136/gutjnl-2017-313923>
- Zhou, K. I., Peterson, B., Serritella, A., Thomas, J., Reizine, N., Moya, S., Tan, C., Wang, Y., & Catenacci, D. V. T. (2020). Spatial and temporal heterogeneity of PD-L1 expression and tumor mutational burden in gastroesophageal adenocarcinoma at baseline diagnosis and after chemotherapy. *Clinical Cancer Research: An Official Journal of the American Association for Cancer Research*, *26*(24), 6453–6463. <https://doi.org/10.1158/1078-0432.CCR-20-2085>
- Zhou, S., Zhu, J., Xu, J., Gu, B., Zhao, Q., Luo, C., Gao, Z., Chin, Y. E., & Cheng, X. (2022). Anti-tumour potential of PD-L1/PD-1 post-translational modifications. *Immunology*, *167*(4), 471–481. <https://doi.org/10.1111/imm.13573>
- Zhou, S. L., Zhou, Z. J., Hu, Z. Q., Huang, X. W., Wang, Z., Chen, E. B., Fan, J., Cao, Y., Dai, Z., & Zhou, J. (2016). Tumor-associated neutrophils recruit macrophages and t-regulatory cells to promote progression of hepatocellular carcinoma and resistance to sorafenib. *Gastroenterology*, *150*(7), 1646–1658.e17. <https://doi.org/10.1053/j.gastro.2016.02.040>

SUPPORTING INFORMATION

Additional supporting information can be found online in the Supporting Information section at the end of this article.

How to cite this article: Rubenich, D. S., Domagalski, J. L., Gentil, G. F. S., Eichberger, J., Fiedler, M., Weber, F., Federlin, M., Poeck, H., Reichert, T. E., Ettl, T., Bauer, R. J., Braganhol, E., & Schulz, D. (2024). The immunomodulatory ballet of tumour-derived extracellular vesicles and neutrophils orchestrating the dynamic CD73/PD-L1 pathway in cancer. *Journal of Extracellular Vesicles*, *13*, e2480. <https://doi.org/10.1002/jev2.12480>